Geomorphology 510 (2026) 110399

Contents lists available at ScienceDirect

Geomorphology

journal homepage: www.journals.elsevier.com/geomorphology

Cave system evolution in dedolomite (central Slovenia)

Filip Šarc [a], Andrzej Tyc [b], Krzysztof Gaidzik [b], Marcin Błaszczyk [c], Tanguy Racine [d], Matej Blatnik [a], Bojan Otoničar [a,*]

[a] Karst Research Institute ZRC SAZU, Titov trg 2, SI-6230, Postojna, Slovenia
[b] Institute of Earth Sciences, University of Silesia in Katowice, Będzińska 60, 41-200 Sosnowiec, Poland
[c] Institute of Geological Sciences, Polish Academy of Sciences, Twarda 51/55, 00-818 Warszawa, Poland
[d] Centre for Hydrogeology and Geothermics, University of Neuchâtel, Rue Emile-Argand 11, 2000 Neuchâtel, Switzerland

ARTICLE INFO

Keywords:
Speleogenesis
Geomorphology
Cave sediments
Geochronology

ABSTRACT

The Mravljetovo brezno v Gošarjevih rupah (MBGR) cave system in central Slovenia provides key insights into the role of dedolomitization in speleogenesis within mixed carbonate–siliciclastic successions. Detailed geomorphological mapping, structural analysis, LiDAR-based morphometry, sedimentology, and U—Th and OSL geochronology were integrated to reconstruct cave and landscape evolution. Dedolomitization acted as an early-stage preconditioning process, enhancing porosity, permeability, and mechanical weakness along bedding planes and fractures, thereby guiding initial conduit development. Cave passages are strongly aligned with Dinaric-oriented fault systems, indicating structural control predating Miocene tectonic reactivation. Morphological features such as ceiling channels, cupolas, rising channels, and pendants reflect a complex interplay between structurally guided phreatic inception and later epiphreatic to vadose modification. U—Th ages up to ~380 ka and OSL-dated sediments at ~87 ka constrains major phases of vadose evolution to at least the Middle Pleistocene, while Holocene speleothems record renewed calcite deposition under stabilized conditions. Progressive uplift and valley incision drove long-term groundwater-level lowering, transitioning the system from phreatic to dominantly vadose conditions. Present morphology is further modified by condensation corrosion linked to active cave ventilation. The MBGR cave demonstrates how dedolomitization can fundamentally influence speleogenetic pathways and highlights caves as valuable archives of tectonic, climatic, and geomorphic evolution in prealpine karst settings.

1. Introduction

Karst caves were initially explained as the product of epigene dissolution in carbonate terrains, where meteoric waters acquire acidity primarily in the form of carbonic acid from soils with elevated pCO_2 driven by microbial respiration (Ford and Williams, 2007; Palmer, 2007). In such settings, meteoric water circulates through the epikarst, vadose, and phreatic zones, enlarging pre-existing voids along bedding planes, fractures, faults or primary porosity. By contrast, waters in deeper crustal environments can be hydrothermal and/or enriched in geogenic or exhalative CO_2 (Klimchouk et al., 2000), and they may carry additional agents like organic acids, CH_4, and particularly H_2S that oxidizes to strong sulfuric acid capable of producing distinct dissolution fabrics and passage morphologies (D'Angeli et al., 2019; De Waele and Gutiérrez, 2022; De Waele et al., 2024). Because multiple agents often operate sequentially or concurrently, caves frequently record overprinting so different processes can yield similar forms, while later phases can obscure or erase earlier ones. Robust reconstruction of speleogenesis therefore requires an explicitly multi-proxy approach that integrates geomorphology with structural geology, petrography/mineralogy, sedimentology, and independent geochronology.

Within this broader context, dedolomitization, i.e. dissolution and replacement of dolomite by calcite in the presence of Ca-rich fluids, can either increase or decrease porosity and permeability (Radwan et al., 2021; Vandeginste and John, 2012) thereby preconditioning rock masses for initial cave formation and later enlargement. Although dedolomitization has been discussed alongside incomplete dissolution and "ghost-rock" karstification (Dubois et al., 2014; Dubois and Quinif, 2019), studies regarding links between dedolomite distribution, passage-scale morphology, and cave evolution remain comparatively sparse.

We address this gap with a case study from the Mravljetovo brezno v

* Corresponding author.
E-mail address: bojan.otonicar@zrc-sazu.si (B. Otoničar).

https://doi.org/10.1016/j.geomorph.2026.110399
Received 19 February 2026; Received in revised form 1 June 2026; Accepted 1 June 2026
Available online 2 June 2026

Gošarjevih rupah (hereafter MBGR) cave in central Slovenia, where decimeter-scale dedolomite remnants are widespread, and passage geometry is maze-like and ramiform (Otoničar et al., 2016; Šarc et al., 2025). Our goal is to test how dedolomitization and its products controlled both the inception and subsequent evolution of the cave. To this end, we (i) map dedolomite relative to the cave passages, (ii) quantify passage morphometry from LiDAR mapping of the almost entire cave system and targeted geomorphological mapping, (iii) characterize cave sediments and wall-rock alteration products, and (iv) use OSL and U—Th geochronology to determine key phases of alteration, enlargement, infill, and speleothem deposition in the cave system. Together, these data allow us to reconstruct superposed processes and propose a model for speleogenesis in dedolomitized dolostones. Since MBGR represents a specific case, its present morphology is the cumulative product of several overprinted phases, i.e., phreatic, epiphreatic, vadose, and the ongoing condensation regimes. Our aim is to determine existing features in detail and compare them with previously described speleogenetic processes to determine whether particular forms record hypogene conditions or instead reflect epigene and epiphreatic processes.

At the same time, caves and their internal records offer exceptional insights into surface geomorphic development. Cave sediments, speleothems, and wall-rock alteration products preserve signals of erosion, transport, and deposition that originate in the wider catchment. In this sense, caves function not only as landforms shaped by subsurface processes but also as natural archives of landscape evolution, recording erosional–depositional dynamics and hydrological regimes which were the main factors in the formation of surface geomorphology.

2. Regional settings

The study area is located near Rovte, some 25 km west of Ljubljana, Central Slovenia (Fig. 1a-b). The study area comprises various carbonate, clastic, and mixed carbonate–siliciclastic geological formations ranging from the Middle Permian to the Middle Triassic (Čar, 2010; Fig. 1c). The Middle Permian Gröden Formation is composed of grey and red shales, siltstones, sandstones, and variegated conglomerates. The Upper Permian successions and the transition to the Lower Triassic rocks feature alternating limestone and dolomite beds, with subsurface layers and lenses of evaporites (gypsum and anhydrite). The transition from Upper Permian to Lower Triassic dolomite is gradual, marked by a shift to lighter grey dolomite with a yellowish hue and increasing fine mica content. The bedded dolomite varies in grain size, appearing sandy and cavernous in some areas, and locally preserves dolomitized ooids. The early Lower Triassic (Induan) Seis beds include grey, green, and red micaceous claystones, shales, siltstones, and sandstones, interbedded with meter-thick layers of oolitic limestones, which are dolomitized in some places. Upwards, the Lower Triassic (Olenekian) Campil dolostones consist of grey, grainy dolomite with thin reddish marly claystone partings. These transition into well-bedded, dark grey Campil marly limestones or marly claystones with variable non-carbonate components of the same thickness. This unit also laterally changes to lithologies characterized by a higher content of non-carbonate clastic material. The Lower to Middle Triassic (Anisian) transition is rather sharp, marked by a horizon of massive to indistinctly bedded fine-grained dark grey dolomite containing millimeter- to centimeter-sized pores and geodes. This is followed by light to medium grey, fine- to medium-grained dolomite, occasionally interbedded with reddish dolomitic siltstone and sandstone. Further up, a horizon of carbonate clastics includes breccias and conglomerates with clasts up to 10 cm in size. In the upper part of these reddish Anisian clastics, a several-meter-thick layer of greyish volcanoclastic deposits is present. Above this sequence, the Ladinian (upper Middle Triassic) limestones are massive and medium grey, containing diploporas and crinoids. West of the study area, particularly on the plateau east of Idrija, coarse-grained to blocky limestone–dolomite conglomerates from the Anisian–Ladinian transition dominate, interbedded with grey and red sandstone, and capped by green tuffs. The Upper Triassic dolomite is one of the most widespread formations south and northeast of the study area (Mlakar, 1969; Čar, 2010; Johnston et al., 2024).

The study area specifically belongs to the Žiri–Trnovo nappe structural unit, part of the External Dinarides (Mlakar, 1969; Placer, 2008). The tectonic evolution includes Middle Triassic deformation, Alpine folding and nappe formation, and Miocene to post-Miocene strike-slip tectonics (Čar, 2010).

The study area lies between two major karst regions: the Dinaric karst to the south and the Alpine karst to the north. According to Gams (2004) and Mihevc et al. (2016), this transitional area belongs to the prealpine or isolated karst. The landscape is characterized by rounded hills and plateaus with numerous closed depressions, dissected by narrow valleys. The highest point in the study area is Vrh Svetih Treh Kraljev (Three Kings Hill) at 884 m a.s.l., while the lowest point, at 486 m a.s.l., is in the Poljanska Sora valley. Along with the MBGR cave, the three most prominent caves in the area, each extending up to 1000 m in polygon length, are Jama pri Sv. Treh Kraljih, Matjaževe Kamre, and Prekov cave (Fig. 1c).

3. Materials and methods

3.1. Cave surveying, mapping and 3D scanning of cave morphology

The current version of the MBGR cave plan was prepared by N. Sznober in 2012, with additions from M. Blatnik and B. Otoničar in 2018, using digital cave survey techniques represented by laser distance, inclination and azimuth measurements with a device called Disto X2 and in-cave drawings. A general outline of the cave passages is presented in Fig. 2a, while details of the MBGR cave morphology are provided in the Results chapter.

Detailed mapping of the cave morphology, distribution of speleogens and sediments, including the zones of dedolomite occurrence, was performed using classical speleological and geomorphological methods. Selected parts of the MBGR cave were documented in detail using a Leica BLK2GO dynamic LiDAR scanner, complemented by a lighting system from Méandre Technologie consisting of five 2250–15,000 lm LEDs arranged around the sensor to provide near-panoramic illumination. Point cloud acquisition followed the workflow described by Racine et al. (2025). Overlaps between acquisitions enabled subsequent co-registration using the ICP algorithm (Besl and McKay, 1992). Point cloud assembly and georeferencing were performed in Cyclone Register 360, and all further cleaning, visualization, and processing were performed in CloudCompare (Girardeau-Montaut, 2016). Ceiling morphologies were analyzed as follows. Ceiling channels were systematically mapped on the point cloud, and cupola to cupola-like sub-spherical forms were identified and classified as individual or composite morphologies. Individual cupolas were manually delineated prior to quantitative analysis.

For each selected cupola, a best-fit sphere was computed using the CloudCompare fitting algorithm. The fitting procedure optimizes the position and radius of the sphere by minimizing the mean distance between the point cloud representing the cupola surface and the fitted geometry. Only clearly defined individual cupolas were included in the statistical analysis, whereas composite morphologies were excluded due to their multi-phase overprinting.

To improve visual discrimination of lithological contrasts, the colored point cloud was further processed in Blender, where increased brightness and rendering adjustments enhanced the visibility of dedolomitized zones relative to surrounding lithologies.

3.2. Structural-geological mapping

Detailed measurements of bedding planes and fractures were conducted at 14 locations within the cave, selected to represent all three

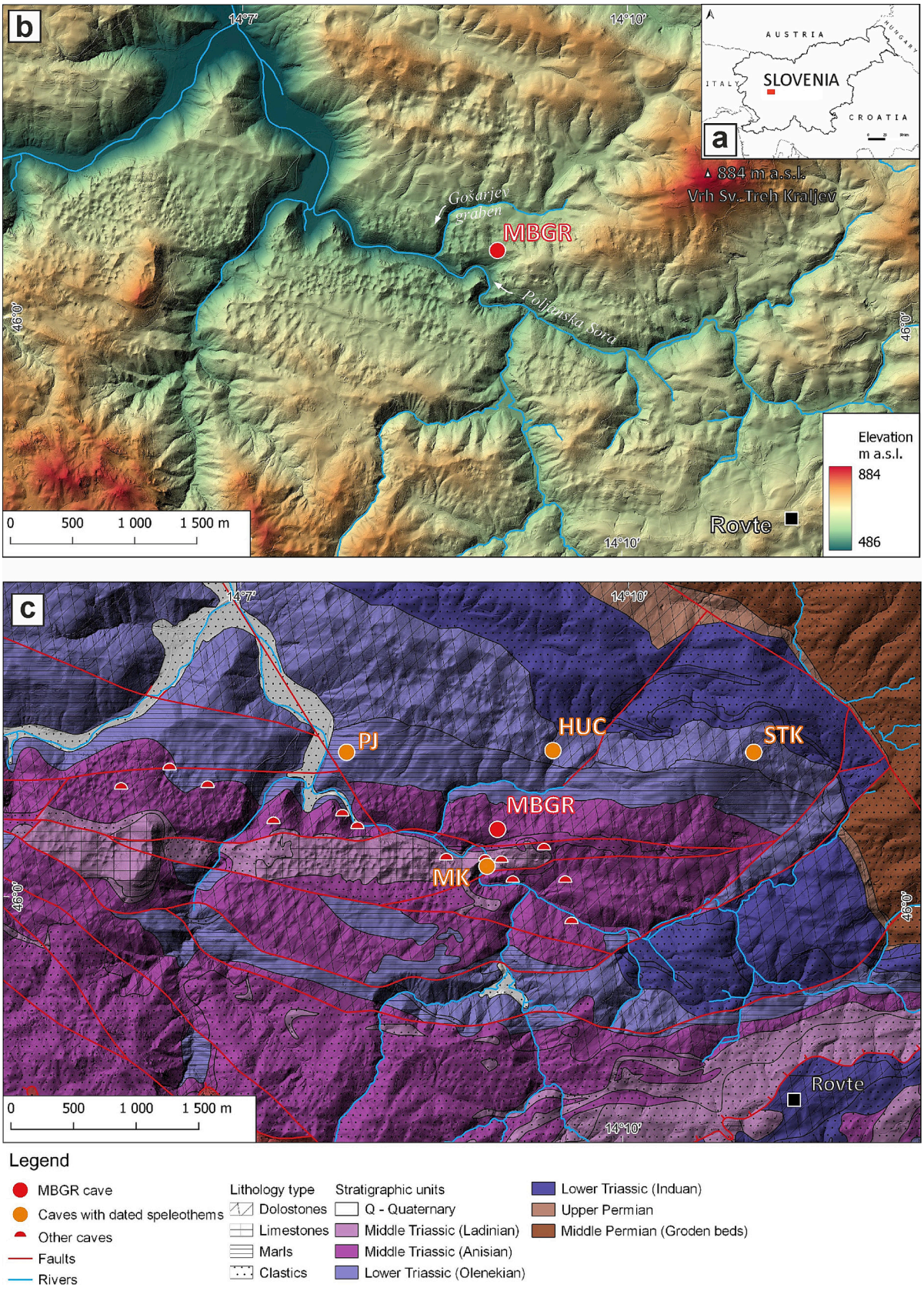

Fig. 1. Study area location. Map of Slovenia indicating the Rovte region (red box) (a); hypsometric map indicating location of the Mravljetovo brezno v Gošarjevih rupah (MBGR) (b); based on the open access digital elevation model (DEM) from the ARSO Geoportal, geological map of the study area (after Johnston et al., 2024, modified) (c), with the indicated location of the main caves (after cave cadaster JZS and IZRK ZRC SAZU), MBGR - Mravljetovo brezno v Gošarjevih rupah, MK - Matjaževe kamre, PJ - Prekova jama, STK – Jama pri Sv. Treh Kraljih and HUC – Hleviše unroofed cave.

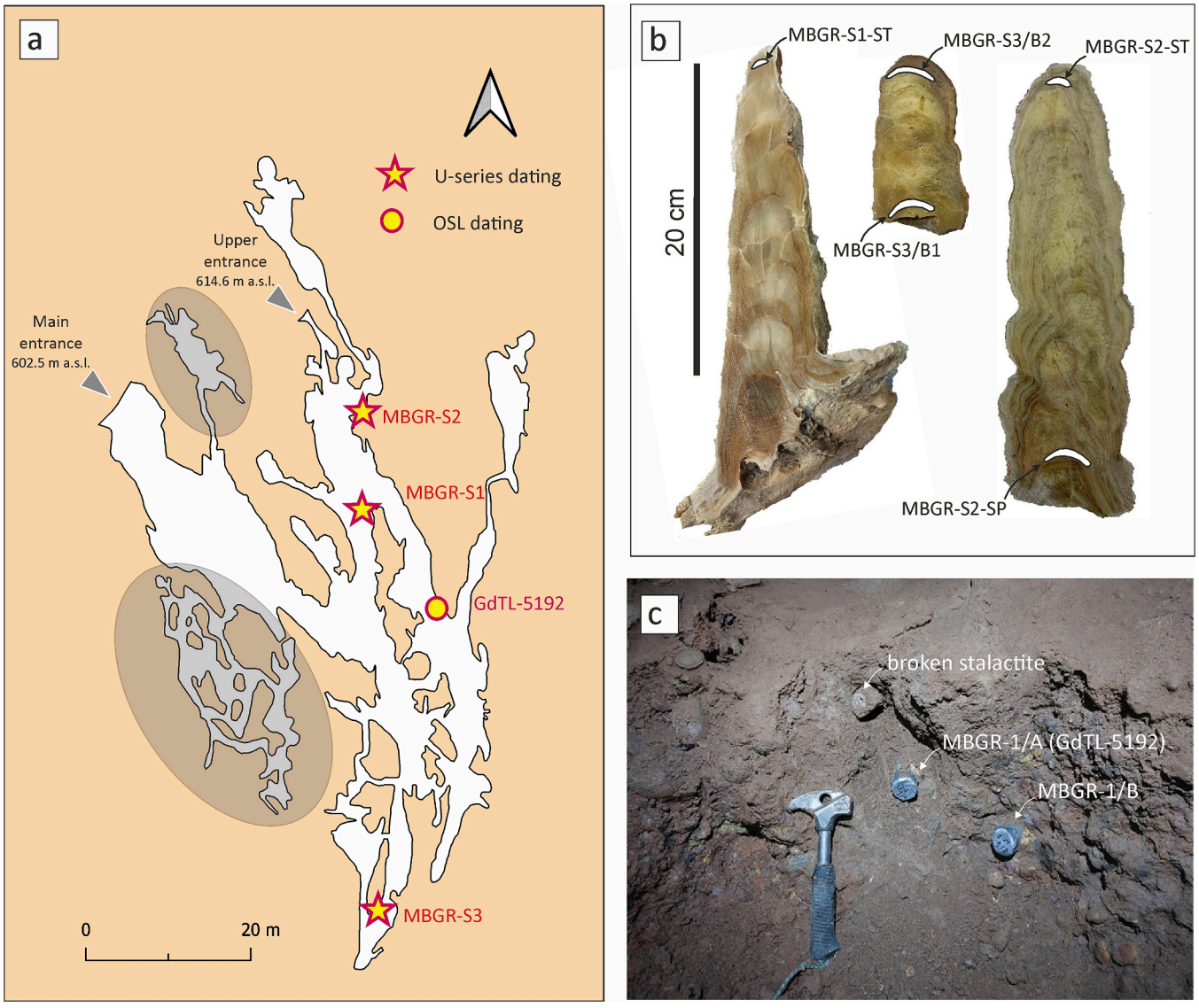

Fig. 2. MBGR cave: general plan view (after Sznober, 2012) and location of samples used for dating (a), shaded parts indicate new cave branches discovered after completion of geomorphological research (after Blatnik and Otoničar, 2018); Speleothem specimens used for U-series dating (b); profile of clastic sediments with the location of sampling sites for OSL dating (c).

main cave levels. The study focused on the geometric, kinematic, and dynamic analysis of minor tectonic deformation structures, including fractures, mesoscale faults with associated surface features and shear indicators, and veins. The study primarily involved the geometric analysis of mesoscale structures, assessing their morphology, spatial orientation, and superpositional relative age relationships. Almost 1500 structural orientation measurements were collected using a Freiberg biaxial geological compass. The data were visualized using structural diagrams (point plots, great circles, and contour stereoplots) in an equal-area Lambert-Schmidt projection on the lower hemisphere, generated with SpheriStat software (Stesky, 1998).

3.3. Clastic cave sediments analysis and OSL dating

To investigate the origin of the MBGR cave sediments, analyses were conducted on clastic sediments present in this cave and two selected caves in the study area: Matjaževe kamre and the cave Jama pri Sv. Trije Kraljih (MK and STK in Fig. 1c, respectively). Additionally, sediments from the Poljanska Sora River and Gošarjev graben stream, as well as soils developed on the Anisian dolomite formation and Lower Triassic marly limestones, were analyzed. Representative rocks of some selected clastic, clastic–carbonate (individual beds within the Anisian dolomite formation), and volcaniclastic formations were also analyzed. Mineralogical composition of clastic sediments, including individual non-carbonate clasts washed out from coarse gravelly sediments in MBGR, soils and rock samples, was performed by powder X-ray diffraction (XRD). All these analyses were conducted at the Karst Research Institute (Research Centre of the Slovenian Academy of Sciences and Arts, Slovenia) using a Bruker D2 PHASER diffractometer (Cu Kα radiation, 30 kV, 10 mA). Samples were scanned in the 2θ range of 3–83° at a scan speed of 0.02° 2θ/0.2 s. Bruker's EVA 5.1 software was used to acquire and process the data.

Granulometric analysis of clastic sediments from the profile in the upper level of MBGR cave (see Fig. 2a,c for location) was performed in the laboratory of the Institute of Earth Sciences of the University of Silesia (Poland) using the classical sieve method. Grain size distribution and associated statistical parameters of the clastic cave sediments were analyzed using GRADISTAT Version 8.0, a Microsoft Excel-based software package. Two samples of clastic sediments from MBGR cave were dated using the optically stimulated luminescence method (OSL) (see

Fig. 2a,c for a location), but only one dating (GdTL-5192) was successful. Samples were collected using 15 cm long polyvinyl chloride (PVC) dark-colored and opaque tubes. Before removing from the sediment profile, the tube was sealed with a layer of aluminum foil on both ends and sealed with opaque tape. The sample was wrapped in opaque black plastic immediately after extraction. Analyses were conducted at the Gliwice Luminescence Laboratory (Silesian University of Technology) in Poland, as detailed by Moska et al. (2021). High-resolution Canberra gamma spectrometry, calibrated with reference materials (IAEA-RGU-1, IAEA-RGTh-1, and IAEA-RGK-1 from the International Atomic Energy Agency), was utilized for dose rate measurements. The equivalent dose determined using the OSL-SAR protocol was 296 ± 11 Gy, based on 15 aliquots analyzed with the Central Age Model. Environmental dose rate calculations, derived from measured activities of Th-232, U-238 and K-40 and corrected for moisture and alpha efficiency, yielded a total dose rate of 3.40 ± 0.11 Gy/ka. These values form the basis of the final age estimate.

3.4. U-series dating

U-series dating was performed for three speleothems from MBGR cave (see Fig. 2a-b). Additionally, one stalagmite from Prekova jama and a fragment of a speleothem from Hleviše unroofed cave (PJ and HUC in Fig. 1c, respectively) were dated. Calcite samples were drilled from both the basal and the youngest growth (top) layers using a high-precision NSK Ultimate XL-GT prosthetic micromotor. Sampling was carried out along laminae with no visible porosity or secondary features, with approximately 500 mg of calcite extracted per sample. The thickness of the drilled samples was typically small, approximately 3 mm, to minimize the temporal averaging of individual analyses.

Chemical preparation of the samples was conducted at the U-series Laboratory of the Institute of Geological Sciences, Polish Academy of Sciences, following the protocol described by Hellstrom (2003). Mass abundances of ^{236}U, ^{233}U, ^{234}U, ^{238}U, ^{229}Th, ^{230}Th and ^{232}Th were measured using a double-focusing sector-field ICP mass spectrometer (Element 2, Thermo Finnigan MAT) at the ICP-MS Laboratory of the Institute of Geology of the Czech Academy of Sciences. Measured values were corrected for background counts and chemical blanks, which were prepared and processed in parallel with the samples. Final results are reported as activity ratios.

U-series ages were iteratively calculated from the $^{230}Th/^{234}U$ and $^{234}U/^{238}U$ activity ratios. All uncertainties, except those associated with decay constants, were incorporated into age uncertainty estimates using standard error-propagation methods. Corrections across the entire profile of twin stalagmites were applied using a modified version of the algorithm proposed by Hellstrom (2006), as further detailed by Błaszczyk et al. (2021).

4. Results

4.1. Geomorphology of the area

The geomorphological diversity of the area reflects its complex lithological composition, consisting of mixed carbonate-siliciclastic units. Thus, the region exhibits characteristics of a fluviokarst landscape (Fig. 3a). The limestone units are associated with the most pronounced relief, characterized by sharp ridges and dense doline networks. Dolostones, on the other hand, have milder morphologies with larger dolines usually elongated along faults, while clastic units have predominantly well-developed fluvial morphologies locally with active water flow. The boundary between Middle Triassic (Anisian) dolostones and Lower Triassic (Olenekian) marly limestones is marked by an irregular contact zone, characterized by traces of blind valleys and stream-sinks (ponors) on the elevated plains (Fig. 3a).

The contact karst zone is divided into two parts by the deep gorge of the Gošarjev graben. Still-active stream-sinks (shown in Fig. 3b) are present in this gorge. Small-scale contact karst has developed at the interface zone between marly limestones and dolostones west of the Gošarjev graben gorge (Fig. 3b). This is evidenced by an occasionally active shallow blind valley terminating at a stream-sink below a permanent spring (Fig. 3b, c). Approximately 200 m downstream of the ponor zone, a 9-m-deep shaft is developed in the dolostones (Fig. 3b, d). East of the gorge, dry valleys are visible in the DEM, with their mouths hanging above the bottom of the latitudinal section of the Gošarjev graben valley (Fig. 3a). This zone of inactive contact karst features, dissected by a stream valley, is located north of the MBGR cave and elongated doline complex.

4.2. Tectonic structures

According to the field measurements and stereoplots, the bedding planes dip toward the southwest at 20–30° (Fig. 4b). There is no significant variation in this trend at the different levels of the cave. A slight change in the strike of the bedding planes is observed from north to south, changing from W–E in the northern part to NW–SE in the southern part. The dip changes from S in the northern part of the cave to SW in the southern part of the cave. No folds were observed or measured in the cave.

More than 1000 fracture measurements were taken at 12 of the 14 sites in the cave (Fig. 4a). This allowed the creation of contour-statistical stereoplots on which groups of fractures with different spatial orientations could be distinguished. Most of the observed fractures are very steeply to vertically inclined (80–90°), as reflected by their concentration near the margins of the stereoplot. Three main fracture strike directions can be identified from the stereoplot: 1) NW-SE, 2) N-S, and 3) NE-SW (Fig. 4c). A group of fractures closer to the center of the stereoplots is parallel to the bedding planes, representing gently dipping bedding fractures. The fractures, oriented NE-SW, are usually filled with mineral veins, representing extensional features that suggest NW-SE extension, and they are also associated with boxwork structures. These fractures are very dense, i.e., up to 10–20 per 5 cm, so they can be characterized as fracture cleavage. Higher-order structures observed in the cave are N-S-directed faults with associated feather fractures.

4.3. Cave morphology

The MBGR cave is formed in Middle Triassic dolostone (Anisian) formation and is located on the karst plateau above Poljanska Sora River (Fig. 1c). The cave has two accessible entrances, located at the southeastern periphery of a large doline complex (Fig. 4a). Its main entrance is located at 602.5 m a.s.l., and the second one at 614.6 m a.s.l. The cave has an officially recorded length of 904 m and a depth of 74 m (Fig. 2a). The cave's morphology is primarily controlled by Dinaric-oriented, north-south-oriented vertical to subvertical faults and bedding planes dipping southwest (Fig. 4). It has maze-like, ramiform morphology with passages on several levels parallel to the inclination of the dolostone bedding and intersected by vadose shafts.

Among the most distinctive cave features are reddish to yellowish dedolomitzation-related material on a large part of the cave walls which we refer to as dedolomite (Fig. 5). In the transition zone between the host rock and the altered rock, there is usually the appearance of boxwork and drusy calcite crystals (Fig. 5b). The floor of the cave passages is largely covered with a thick layer of flat blocks of dedolomite (Fig. 6). Except for vadose shafts and passages with active water flow, dedolomitization-related material is present in almost the whole cave system (Fig. 7).

The surface of the cave walls covered with dedolomitization-related material is extremely irregular, characterized by numerous bumps and cavities. The contact zone between the dolostone and the dedolomitization-related material exhibits the highest porosity, making it particularly susceptible to weathering. As a consequence, gaps commonly develop along this contact. In addition to the dedolomite,

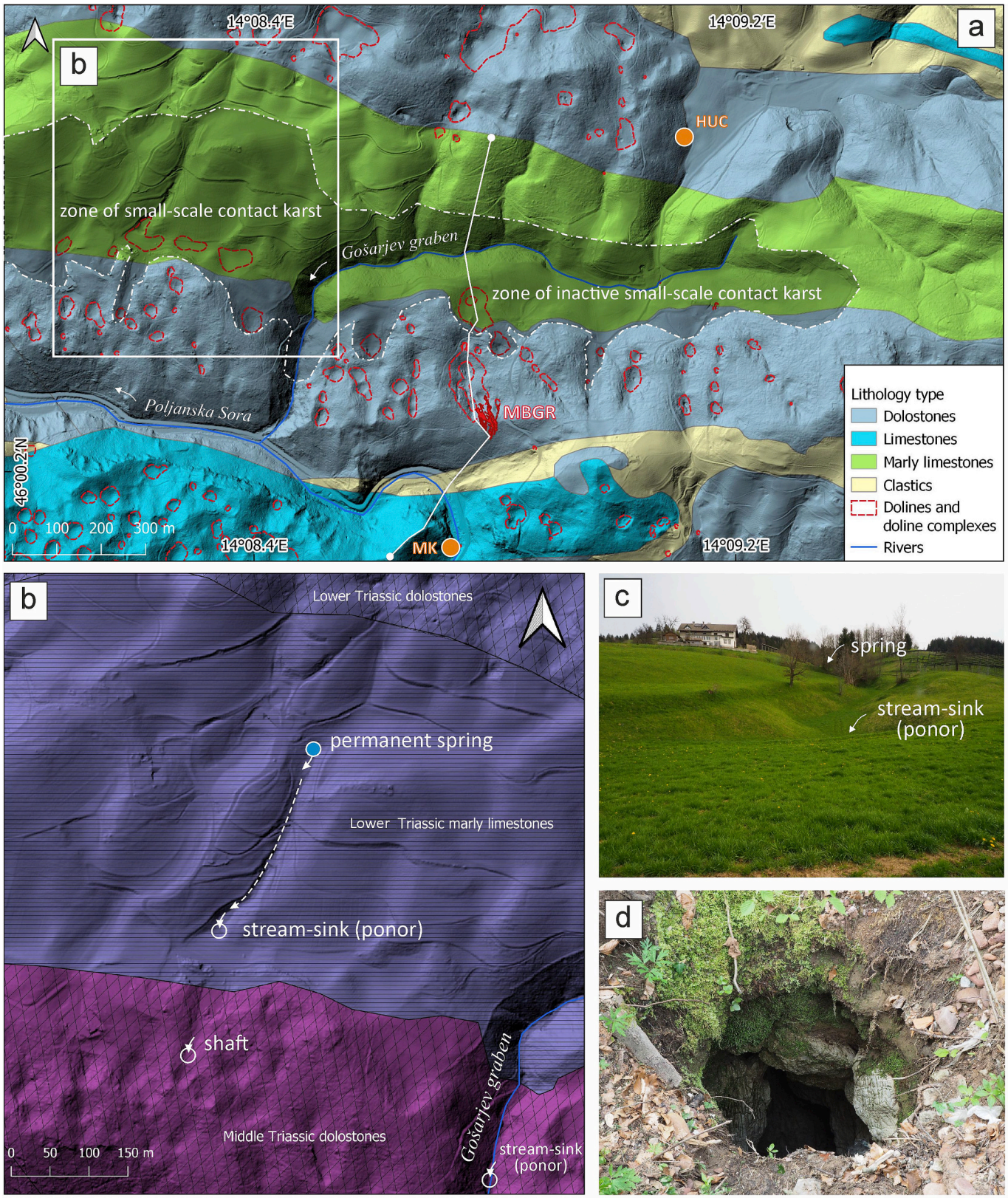

Fig. 3. The main features of the karst relief of the study area (a), based on the digital elevation model (DEM) and geological map (see Fig. 1 for explanation), broken line shows the location of the geological cross-section used in Fig. 8; small-scale contact karst in the Izgorje (b, location as rectangle in Fig. a); upper part of blind valley (c); shaft (d).

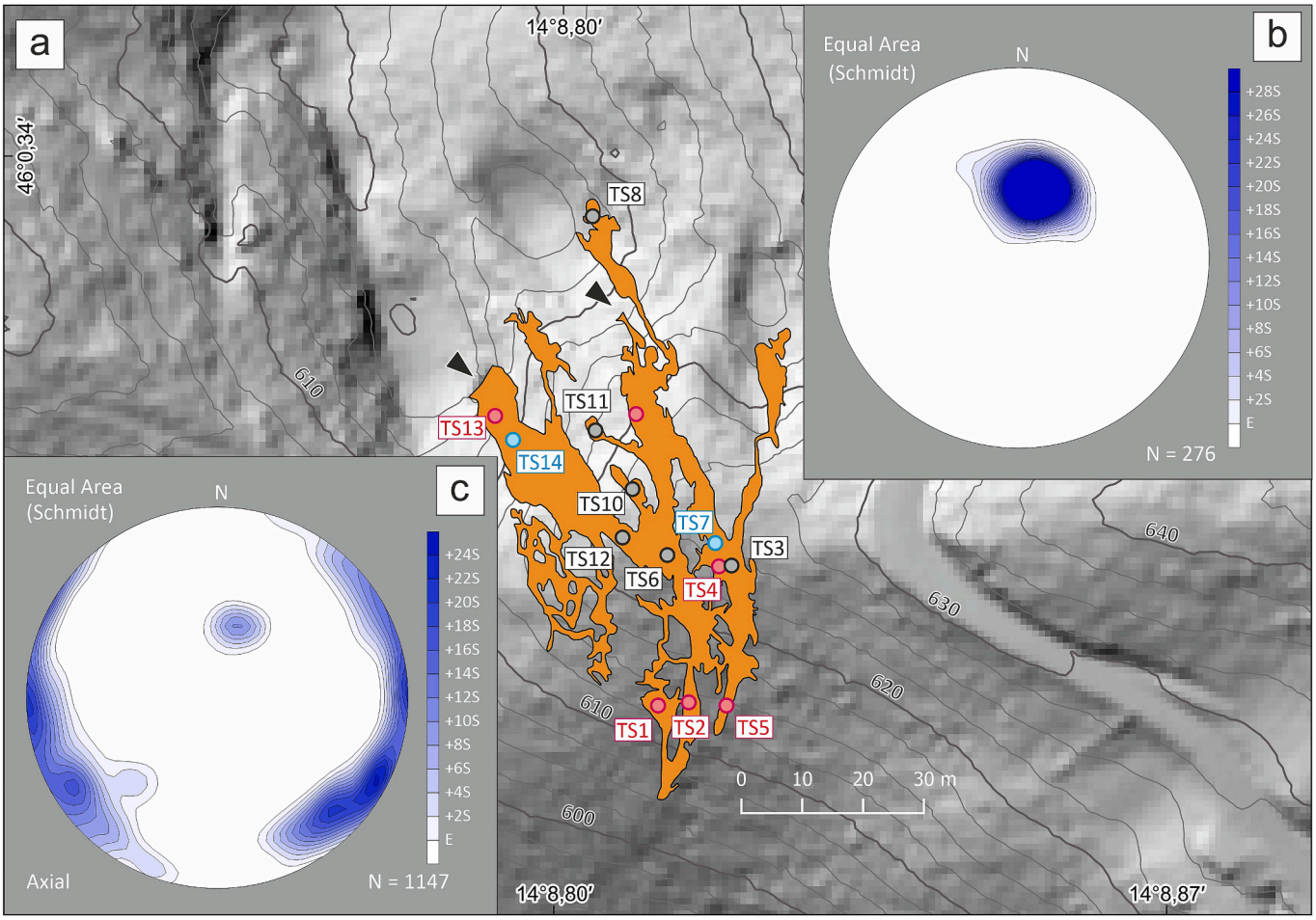

Fig. 4. Location of structural measurement sites in the MBGR cave (a), colour of the circles indicates the cave level - upper (blue), middle (black), lower (red); spatial orientation of bedding (b) and brittle meso-structures, including fractures and faults, (c).stereoplots, projected onto the upper hemisphere, were generated using SpheriStat software (Stesky, 1998).

several characteristic ceiling morphologies are observed (Fig. 6). Ceiling channels are the most common forms and exhibit a winding, sinuous geometry; their width generally does not exceed 0.5 m (Fig. 6a,b,d,f). Along the same fissures, vertical tubular forms occur as rising channels, often arranged in series (Fig. 6c). Cupolas are also present and display well-developed spherical to ellipsoidal shapes, with diameters ranging from approximately 0.5 m to several meters (Fig. 6e). They are commonly elongated along fissures or faults and are frequently connected to ceiling channels. Locally, pendants occur between adjacent ceiling channels as residual forms (Fig. 6f,g).

The LiDAR survey of the cave system (Fig. 8a) allows the morphologies described above to be visualized in their full geometric context and significantly enhances the interpretation of their spatial distribution and relationships to structural elements such as faults and bedding planes (Fig. 8b,c). This approach allows the previously described cave wall and ceiling features, e.g. ceiling channels (Fig. 8d) and cupolas (Fig. 8e) to be visualized in 3D and facilitates assessment of their spatial distribution and geometry. In addition to these dominant forms, other morphologies are also clearly resolved in the LiDAR data, including rising channels and pendants that decorate the ceilings (Fig. 6b, c). The three-dimensional representation reveals strong structural control on the development of these features: ceiling channels preferentially follow bedding planes, whereas vertical elements, such as rising channels and elongate cupolas are aligned with fracture and fault zones. The systematic elongation of cupolas along fractures further highlights the role of tectonic discontinuities in controlling their geometry and orientation.

Morphometric, LiDAR-based analysis reveals a well-developed network of ceiling channels associated with numerous cupola to cupola-like morphologies distributed throughout the surveyed volume (Fig. 9a). A total of 55 individual cupolas were identified, along with several composite features where multiple generations of cupolas overlap.

The fitted sphere radii range from 0.14 m to 1.86 m, with a mean of 0.8 m (standard deviation = 0.4 m; median = 0.66 m; $n = 55$). The size distribution is approximately log-normal, characterized by a high frequency of small cupolas and progressively fewer larger ones. The observed bias toward smaller radii likely reflects incomplete sampling of the smallest morphologies.

The enhanced visualization of the point cloud highlights clear lithological contrasts, particularly the spatial association between dedolomitized zones and the mapped ceiling morphologies (Fig. 9b, c).

The MBGR cave currently lies within shallow subsurface vadose conditions. Entrances located in the upper part of the system and their vertical difference contribute to a chimney effect, creating a bimodal cave microclimate that facilitates intensive air exchange between the surface and the cave. This results in the influx of warm, humid air and cold, dry air, leading to condensation corrosion and evaporation-driven processes, respectively. These conditions are dominant in the upper parts of the cave, whereas in the lower sections, the primary controlling factor is flowing vadose water, which eventually disappears at the bottom of the cave.

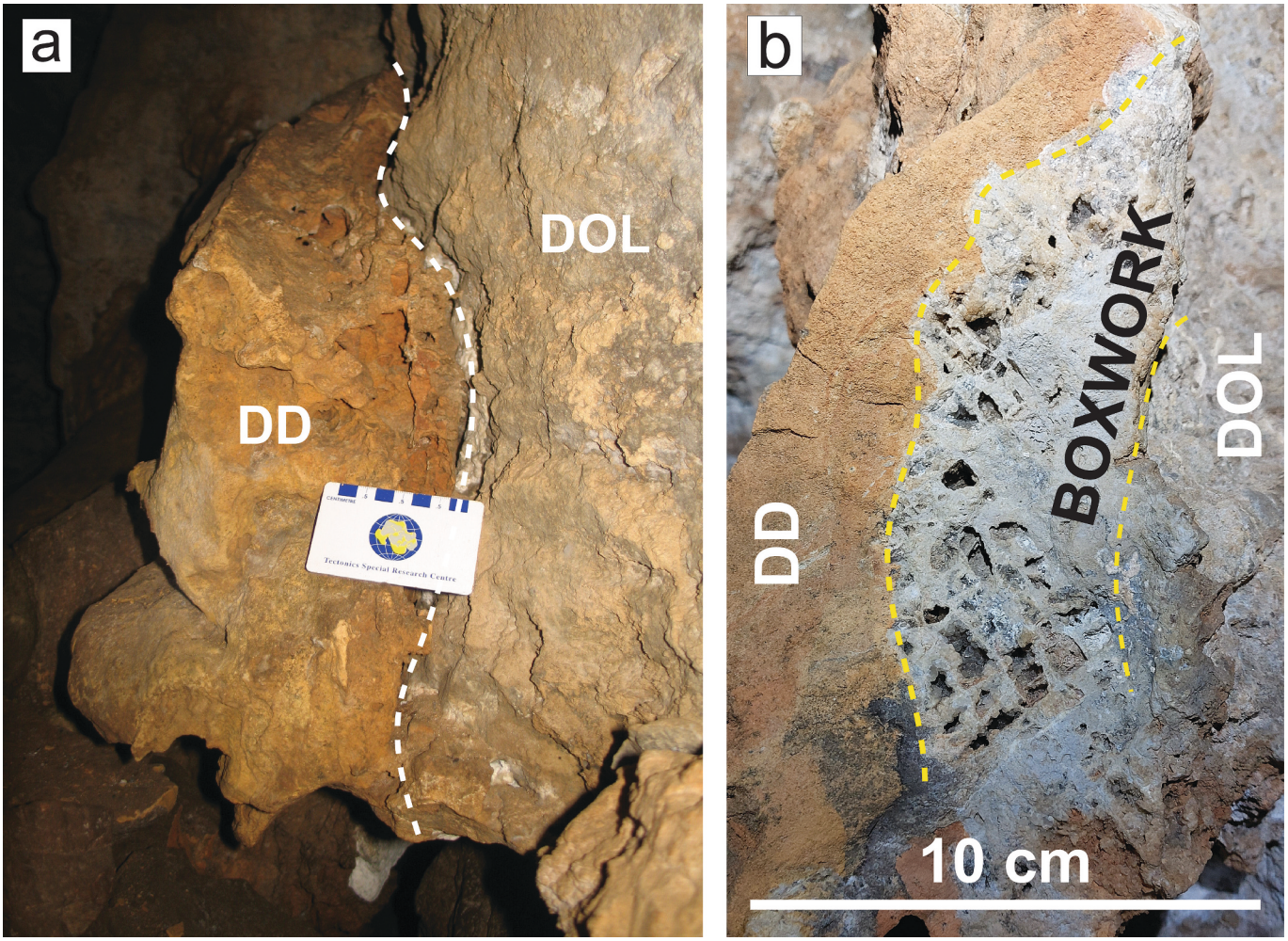

Fig. 5. Occurrence of dedolomitization-related material in the MBGR cave; (a) transition from dolostone – DOL to dedolomite – DD (from right to left), (b) boxwork with drusy calcite usually occurring in the transition zone from dolostone – DOL to dedolomite – DD.

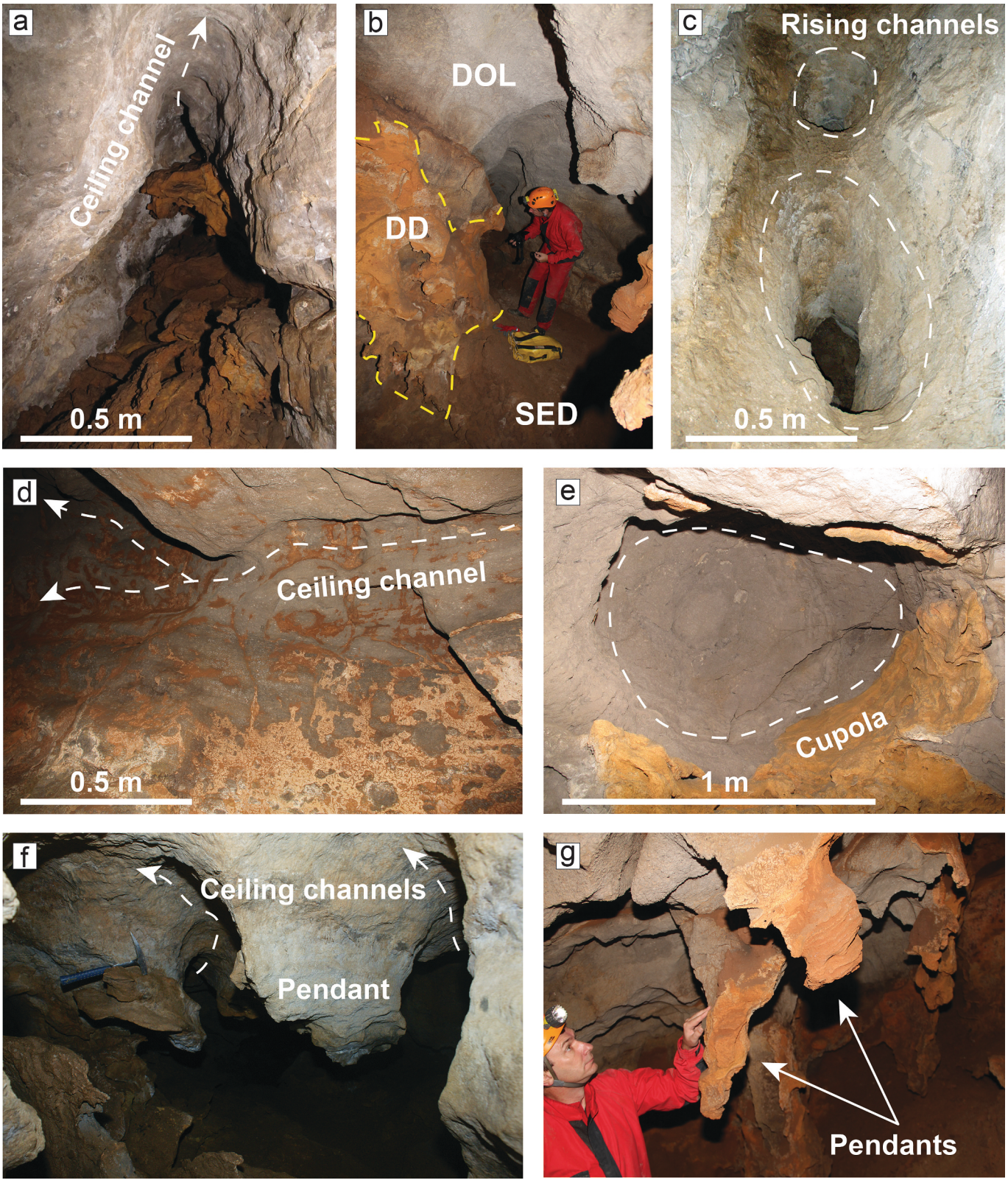

Fig. 6. Cave wall and ceiling morphologies associated with dedolomitization-related material: (a) irregular cave wall surface with a well-developed ceiling channel carved into dolostone and dedolomite, (b) contact zone between dolostone (DOL) and dedolomitization-related material (DD), showing highly irregular surface; SED = cave sediment, (c) rising channels developed along a fissure, forming a tubular conduit (d) sinuous ceiling channel, (e) cupola with a spherical to ellipsoidal shape, (f) pendant preserved as a residual form between adjacent ceiling channels, (g) multiple pendants developed beneath the ceiling as remnant forms related to preferential dissolution.

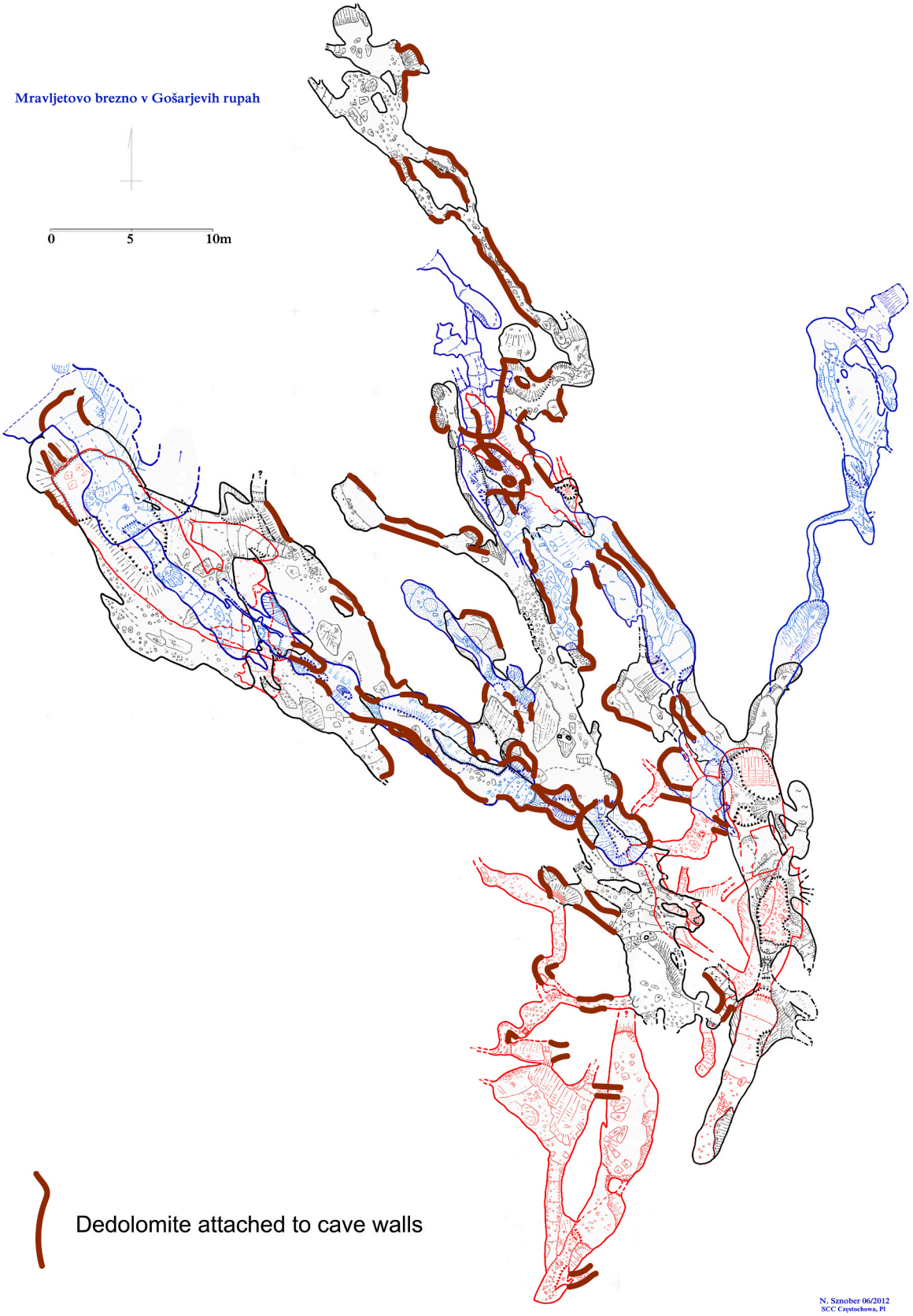

Fig. 7. Cave map showing widespread distribution of dedolomite (brown) on passage walls in Mravljetovo brezno v Gošarjevih rupah. Scale bar: 0–10 m.

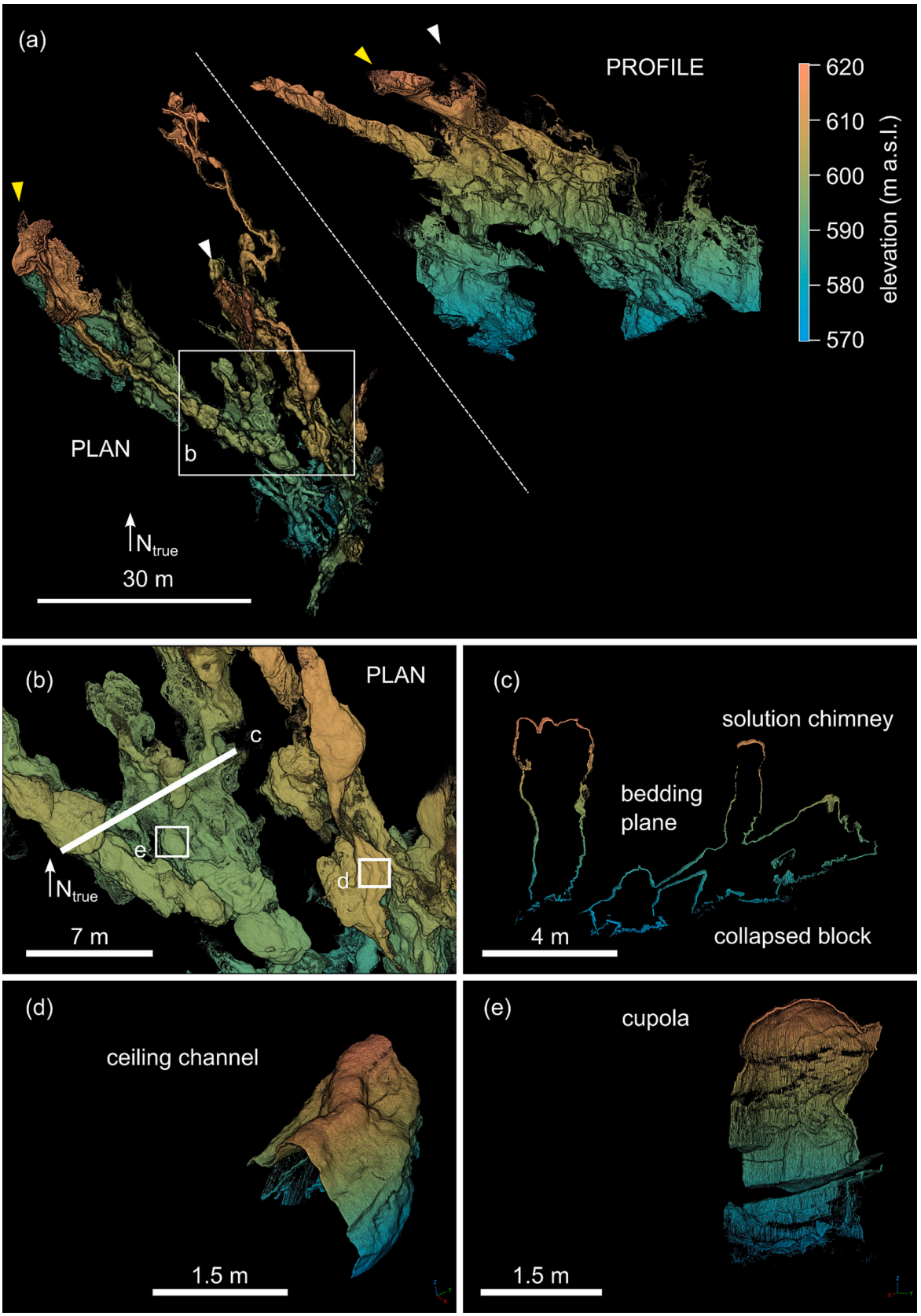

Fig. 8. LiDAR-based 3D model of the MBGR cave system showing the spatial distribution and morphology of speleogenetic features: (a) LiDAR scan of a part of the cave, illustrating the overall passage geometry, (b) detailed view of the "Central Hall", showing the complex arrangement of channels and ceiling morphologies, (c) cross-section showing the relationship between structural features and the geomorphology of the cave, (d) detail of a ceiling channel, (e) detail of a ceiling cupola exhibiting a nearly spherical shape. Scene shown on (b) is marked with a rectangle on (a), whereas a cross-section shown on the (c) is marked with a line on the (b). The lower cave entrance is marked with a yellow arrow, while the upper entrance is marked with a white one.

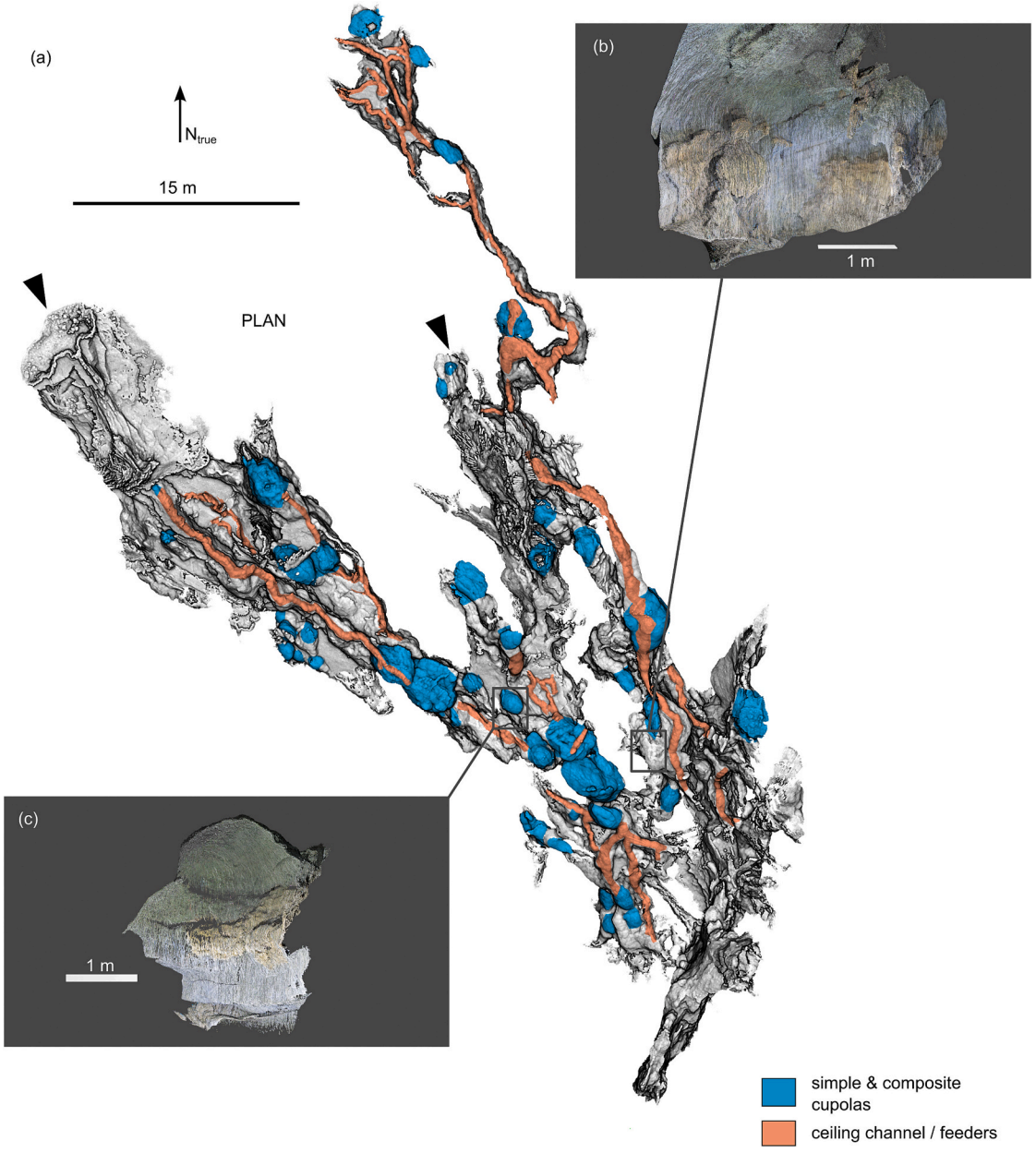

Fig. 9. Plan-view representation of the LiDAR-derived cave model showing mapped ceiling morphologies. Ceiling channels are highlighted in orange, while individual and composite cupola to cupola-like (sub-spherical) forms are shown in blue. Insets (b) and (c) present representative cupola morphologies derived from the point cloud (scale bars = 1 m). The model is oriented to true north; the main scale bar represents 15 m. Colour-enhanced rendering emphasizes lithological contrasts, particularly dedolomitized zones. The cave entrances are marked with black arrows.

4.4. Clastic cave sediments

The clastic cave sediments analyzed are characterized as polymodal and poorly sorted, consisting predominantly of very coarse sandy gravel (Fig. 2c). According to clastic cave-sediment terminology, this lithofacies corresponds to a diamicton facies and, based on its granulometric and textural properties, indicates deposition related to debris-flow processes (Bosch and White, 2007; Gillieson, 1986; Robu et al., 2026). The grain size distribution plot confirms a wide range of particle diameters, highlighting significant textural immaturity and the presence of mechanical weathering processes. Semiquantitative X-ray diffraction (XRD) analysis of the 2 samples of the sandy fraction shows that in one sample, clay minerals (50%), quartz (40%), and dolomite (10%) are present. In the second sample, quartz is dominant (40%), followed by clay minerals (34%) and dolomite (27%). XRD analysis of three individual clasts from the same sedimentary body indicates quartz as the dominant phase, accompanied by clay minerals; it is also important to note that the clasts are extremely soft and highly weathered. Although there are indications that the clasts may be of igneous origin, they are too weathered to allow confident lithological identification. In addition, a decimeter-sized block located at the very bottom of the cave was analyzed. This block is not part of the studied sedimentary body, but it may represent material deposited by the same event. Semiquantitative XRD analysis indicates a mineralogical composition of approximately 55% plagioclase, 33% quartz, 9% mica, and 3% clay minerals, which suggests a mineralogical composition consistent with a basic igneous rock. Similar to the mineralogy of the MBGR cave, sediments from the adjacent Matjaževe kamre cave, as well as sandy fluvial sediments of the Sora river, contain plagioclases. Sediments from the Jama pri Sv. Trije Kraljih cave exhibit a somewhat different mineralogical composition. The feldspar fraction consists exclusively of K-feldspar, with the exception of a single sample in which plagioclase is the only feldspar present; in this case, an individual pebble was analyzed.

Luminescence dating of a sample of siliciclastic cave sediment (lab code GdTL-5192) produced an OSL age of 87.0 ± 4.2 ka.

4.5. Speleothem U/Th geochronology

U-series dating was performed on six calcite samples drilled from three stalagmites in the MBGR cave system (Table 1 and Fig. 2b). From the top part of a stalagmite, sample MBGR-S1-ST provided the oldest age of 380 + 48/−34 ka. For the basal part of the same stalagmite MB-S1SP, no corrected age could be obtained. Sample MBGR-S2-SP, which represents the base of stalagmite yielded an age of 8.54 + 0.34/−0.33 ka. Sample MBGR-S2-ST, which represents the top of the stalagmite, yielded a slightly younger age of 5.62 + 0.39/−0.38 ka. The final two samples, MBGR-S3/B2 and MBGR-S3/B1, were collected from different sections of the MBGR-S3 stalagmite. They yielded ages of 10.53 ± 0.31 ka and 10.86 ± 0.29, respectively.

From the Hleviše unroofed cave, two calcite samples (Table 1) (HL-SIG-1 and HL-SIG-2) yielded ages of 420 + 91/−50 ka and 340 + 26/−21 ka, respectively. Two samples from a single speleothem from the Prekova cave produced ages of 159 + 2.3/−2.2 ka (PREK-1-SP, basal part) and 128 ± 1.6 ka (PREK-1-ST, upper part).

5. Discussion

5.1. Geomorphology of the cave system in dedolomite

The dedolomitization features observed in the MBGR cave system indicate that this diagenetic process acted as an early-stage rock alteration that preconditioned subsequent speleogenesis. By increasing porosity, permeability, and mechanical weakness along fractures and bedding planes, dedolomitization facilitated later passage enlargement. It thus represents a fundamental preconditioning factor, enhancing rock heterogeneity and dissolution potential (Otoničar et al., 2016; Šarc et al., 2025). Dedolomitization is a coupled dissolution–precipitation process in which dolomite dissolves under Ca-rich meteoric conditions and is progressively replaced by calcite. During the initial stages, dissolution along crystal boundaries and micro-defects creates a porous framework, while calcite begins to precipitate within this evolving pore system. This interplay can locally produce residual skeletal networks and cavities filled by calcite, which are expressed macroscopically as boxwork structures (Šarc et al., 2025).

The subsequent evolution of this process is recorded by the different dedolomite types described in previous studies (Šarc et al., 2025). Type 1 represents the earliest stage, where dissolution and calcite precipitation occur simultaneously, producing textures of partially replaced dolomite with “floating” dolomite grains in calcite cement and abundant porosity. Type 2 reflects a more advanced stage, characterized by complete replacement of dolomite by calcite, often accompanied by iron oxides and detrital material. Type 3 differs in being a detrital facies, formed by the reworking, transport, and redeposition of weathered host dolomite and dedolomitized material within the cave under low-energy conditions (Šarc et al., 2025).

Previous research indicates that dedolomitization most likely occurred in low-energy phreatic conditions involving meteoric water

Table 1
U—Th dating results for six calcite samples drilled from stalagmites of the MBGR cave, Hleviše unroofed cave and Prekova cave. Reported are uranium concentrations (U conc.), measured activity ratios ($^{234}U/^{238}U$, $^{230}Th/^{234}U$, $^{230}Th/^{232}Th$), uncorrected ages, corrected ages with 2σ uncertainties, and initial $^{234}U/^{238}U$ activity ratios. Corrected ages are calculated after correction for detrital contamination, following the procedure of Hellstrom (2006).

Sample	U cont. [ppm]	$^{234}U/^{238}U$ AR	$^{230}Th/^{234}U$ AR	$^{230}Th/^{232}Th$ AR	Age [ka]	Corr. Age [ka]	$^{234}U/^{238}U$ AR ini.
Hleviše unroofed cave							
HL-SIG 1	0.411 ± 0.003	1.045 ± 0.0035	0.994 ± 0.012	129.8 ± 1.7	420^{+91}_{-50}	$\mathbf{420}^{+91}_{-50}$	1.147 ± 0.046
HL-SIG 2	0.431 ± 0.004	1.034 ± 0.0025	0.966 ± 0.009	54.3 ± 0.51	342^{+26}_{-21}	$\mathbf{340}^{+26}_{-21}$	1.088 ± 0.019
Mravljetovo brezno v Gošarjevih rupah (MBGR) cave							
MBGR-S1-ST	0.281 ± 0.003	1.048 ± 0.003	0.985 ± 0.011	362.1 ± 3.9	382^{+45}_{-33}	$\mathbf{380}^{+48}_{-34}$	1.142 ± 0.039
MBGR-S2-SP	0.472 ± 0.004	1.056 ± 0.003	0.077 ± 0.002	34.71 ± 0.82	$8.76^{+0.22}_{-0.22}$	$\mathbf{8.54}^{+0.34}_{-0.33}$	1.057 ± 0.004
MBGR-S2-ST	0.471 ± 0.004	1.053 ± 0.003	0.053 ± 0.002	14.67 ± 0.38	$5.94^{+0.17}_{-0.17}$	$\mathbf{5.62}^{+0.39}_{-0.38}$	1.054 ± 0.004
MBGR-S3/B2	0.466 ± 0.004	1.026 ± 0.003	0.093 ± 0.002	65.6 ± 1.5	$10.75^{+0.26}_{-0.26}$	$\mathbf{10.53}^{+0.31}_{-0.31}$	1.026 ± 0.004
MBGR S3/B1	0.445 ± 0.004	1.029 ± 0.003	0.095 ± 0.002	105.1 ± 2.2	$10.99^{+0.25}_{-0.25}$	$\mathbf{10.86}^{+0.29}_{-0.29}$	1.03 ± 0.004
Prekova jama							
PREK-1-SP	0.979 ± 0.008	1.271 ± 0.003	0.799 ± 0.005	1587 ± 11	$159^{+2.3}_{-2.2}$	$\mathbf{159}^{+2.3}_{-2.2}$	1.424 ± 0.009
PREK-1-ST	0.782 ± 0.007	1.393 ± 0.003	0.721 ± 0.005	2427 ± 18	$128^{+1.6}_{-1.6}$	$\mathbf{128}^{+1.6}_{-1.6}$	1.564 ± 0.009

SP – base, ST – top of the stalagmite.

enriched with soil-derived CO_2. The process was accompanied by the input of external detrital material. Detrital material in dedolomite comes from surface-derived sediments and from weathering of the host rock, transported into the fractured zones by percolating water. It includes siliciclastic particles like quartz and clays, as well as carbonate fragments (Šarc et al., 2025). The resulting dedolomite bodies consist of lithologies with varying degrees of porosity and cementation, producing a highly heterogeneous rock mass. Such conditions resemble those described in ghost-rock karstification models, where early chemical alteration weakens the rock prior to mechanical removal and passage formation (Dubois et al., 2014; Dubois and Quinif, 2019). Dedolomitization, ghost-rock formation, and recrystallization should be distinguished primarily by their dominant mechanism, even though in natural carbonate systems they may texturally and genetically overlap (Folk, 1965; Bathurst, 1975; Tucker and Wright, 1990). Dedolomitization is best understood as the net calcitization of dolomite, that is, replacement of dolomite by calcite (Evamy, 1967). It may occur either by relatively direct replacement, close to volume-conservative pseudomorphic substitution, or by a two-step pathway involving partial dissolution of dolomite followed by contemporaneous or subsequent precipitation of calcite within the newly created pore space (Al-Hashimi and Hemingway, 1973; Evamy, 1967; Nader et al., 2008). Accordingly, dedolomite may preserve the original dolomitic fabric well, including pseudomorphic or semipseudomorphic textures, but in other cases may show more drusy or cement-like calcite where dissolution played a stronger role (Evamy, 1967). In contrast, ghost-rock formation is fundamentally a dissolution-residual process: selective dissolution weakens the rock and creates a porous in-situ framework that still preserves the original architecture, at least temporarily, before later collapse, erosion, removal of loosened particles (Dubois et al., 2014). Also ghost rock could be later completely or partly cemented (Dubois et al., 2014). Thus, the key distinction is that ghost rock is governed mainly by fabric-preserving dissolution and residual weakening, whereas dedolomitization is governed mainly by replacement of dolomite by calcite, even where dissolution and pore-filling calcite are involved (Dubois et al., 2014; Evamy, 1967; Tucker and Wright, 1990). Recrystallization or neomorphic alteration differs from both because it involves calcite-to-calcite transformation, that is, reorganization of crystal size and fabric without the essential mineralogical change as when dedolomitization is in question (Folk, 1965; Bathurst, 1975; Flügel, 2004). Its typical expression is the aggrading transformation of fine micritic calcite into microspar or spar through fluid-mediated dissolution and reprecipitation driven by reduction of surface energy and stabilization of larger crystals (Folk, 1965; Bathurst, 1975; Tucker and Wright, 1990; Flügel, 2004). In practice, these categories are best treated as end members of a diagenetic continuum, and petrographic description should therefore identify both the dominant process and any superimposed overprint, for example dedolomitization over a ghost-rock-like precursor fabric, or dedolomitized limestone subsequently modified by neomorphic recrystallization (Bathurst, 1975; Tucker and Wright, 1990; Flügel, 2004; Dubois et al., 2014). More generally, dedolomitization is commonly associated with near-surface meteoric environments related to karst processes (Kenny, 1992; Raines and Dewers, 1997; Zeeh et al., 2000; Ronchi et al., 2004; Cantrell et al., 2007; Nader et al., 2008; Hauck et al., 2018; Liu et al., 2021).

The dedolomitization process implies an external supply of Ca-rich fluids. Elevated Ca^{2+} activity promoted calcite supersaturation and, through the common-ion effect, favored dissolution of dolomite together with replacement by calcite and local precipitation of calcite cement. The observed textures therefore indicate an open-system diagenetic environment with surplus calcium availability (Evamy, 1967; Bischoff et al., 1994; Palmer, 2007). Although the precise source of calcium required for the dedolomitization remains uncertain, two principal mechanisms are considered. The first involves deep sulfate-rich artesian waters documented in regional wells, where sulfate derived from evaporite dissolution may have promoted dedolomitization under suitable geochemical conditions (Philipp, 2015). The second possibility is the dissolution of secondary gypsum formed within adjacent pyrite-rich marly limestones. Alternative sources, such as soil-derived solutions or dissolution of surrounding limestones, cannot be entirely excluded (Nader et al., 2008).

Features in the MBGR cave system such as cupolas, ceiling channels, pendants, rising channels and chimneys raise fundamental questions about fluid pathways, hydraulic conditions, and geochemical environments during speleogenesis. Although their exact mechanism of formation in the MBGR cave system is not unequivocally evident, three principal genetic scenarios may account for their origin: (1) hypogene speleogenesis driven by ascending fluids related to the dedolomitization, (2) epigene development under epiphreatic conditions, and (3) paragenetic modification associated with sediment-filled passages and upward-shifted dissolution.

5.1.1. *Hypogene process*

Because dedolomitization is sometimes associated with sulfate dissolution and the common-ion effect, it has occasionally been interpreted within a hypogene speleogenetic framework (Back et al., 1983; Palmer, 2007). Hypogene cave systems are typically formed by rising fluids under hydraulic pressure, often producing distinctive morphologies such as cupolas, ceiling channels, and chimney-like feeders (Klimchouk, 2009; Audra and Palmer, 2015). In the MBGR cave system, several ceiling and wall features, including channels, cupolas, and rising channels and chimneys (the so-called “morphological suite of rising flow”), were therefore evaluated in light of this hypothesis.

According to the criteria proposed by Klimchouk (2009), the MBGR cave system partially satisfies two indicators of hypogene speleogenesis. Regionally, sulfate-rich artesian waters occur in local wells (Philipp, 2015), suggesting that deep-seated fluids may have circulated in the broader area. Nevertheless, a direct hydrological connection between these deep waters and the MBGR caves has not been demonstrated. The second criterion concerns previously described ceiling cave morphologies. However, cave sediments, mineral assemblages, and wall-rock geochemistry do not show clear evidence of hydrothermal and/or high-pressure fluids or strong acids involvement (Šarc et al., 2025).

Thus, while some regional and morphological observations may be compatible with a hypogene contribution, conclusive geochemical and sedimentological indicators are lacking. In addition, the data suggest that dedolomitization and cave formation are distinct stages and likely formed under different conditions.

5.1.2. *Epigene epiphreatic process*

Ceiling morphologies are not exclusive to hypogene environments. Similar forms may develop in epigene settings under specific hydrological conditions. In particular, repeated water-table fluctuations in epiphreatic conditions may localize corrosion near ceilings, generating cupola-like cavities and upward-elongated features (Audra and Palmer, 2011, 2015; Gabrovšek et al., 2014).

In such settings, dissolution concentrates near the fluctuating phreatic surface, where corrosion and renewed undersaturation enhance wall and ceiling dissolution. This mechanism provides a plausible explanation for certain upward-oriented morphologies in the MBGR cave system without invoking deep-seated ascending fluids.

5.1.3. *Antigravitative erosion (paragenesis) in epigene settings*

Antigravitative erosion (paragenesis) offers a further explanation for ceiling features. Sediment accumulation on passage floors can force flowing water upward, shifting dissolution toward ceilings and upper walls and producing characteristic paragenetic forms (Zupan Hajna et al., 2008; Pasini, 2009; Cooper and Covington, 2020; De Waele and Gutiérrez, 2022). Under such conditions, ceiling channels and cupolas may form as a direct consequence of sediment-controlled flow confinement. The zone of small-scale contact karst (Fig. 3) may indicate the occurrence of this process and represent a potential source of the eroded

material. Given these premises and the observed cave features, this mechanism appears to be the most plausible explanation.

Regardless of the exact origin of the initial alteration, it is evident that dedolomitized zones later guided epigene cave development. Surface-derived waters exploited the pre-weakened structural pathways and progressively enlarged them into cave passages (Šarc et al., 2025). The preserved dedolomite most likely represents the better-cemented fraction of the altered zone, whereas less cemented and more porous material was preferentially removed during cave development. Cementation related to dedolomitization was heterogeneous, resulting in strong contrasts in hardness and resistance to weathering within the altered zones (Dubois et al., 2014; Šarc et al., 2025). The best-preserved dedolomite commonly occurs along the margins of fracture zones, where calcite cementation was most intense at the contact with the host dolostone. At the same time, these marginal zones also show the highest porosity due to particularly intensive dolomite dissolution (Šarc et al., 2025). Subsequent regional uplift shifted the hydrogeochemical regime from phreatic to epiphreatic and eventually vadose conditions. Undersaturated meteoric waters dissolved both dolomite and calcite; however, due to kinetic differences, calcite (the principal component of dedolomite) dissolves more rapidly than dolomite, even when both are undersaturated (Ford and Williams, 2007).

As a result, cave morphology partly reflects the original geometry of the dedolomitized bodies and partly records their irregular dissolution, controlled by internal variations in porosity and permeability. Present-day microclimatic processes further complicate the interpretation. Although the cave lacks a geothermal heat source, the vertical difference between its entrances induces a chimney effect that drives seasonally dependent air circulation (Dreybrodt et al., 2016; Columbu et al., 2021; Kukuljan et al., 2021). Condensation during warm periods and freezing processes during cold periods do not generate primary ceiling morphologies, but they clearly modify and reshape pre-existing forms.

5.2. Tectonic setting of the cave system

The tectonic setting of the MBGR cave system is complex due to its location in the frontal part of the Outer Dinarides over-thrust zone (Trnovo Nappe) and within the Idrija Fault zone (Mlakar and Čar, 2009; Čar, 2010). This results in a complex system of faults and fractures, belonging to at least three distinct fault sets and accompanying shears and joints: Dinaric orientation (NW-SE), cross-Dinaric orientation (NNE-SSW), and N-S striking faults (Čar and Gospodarič, 1983; Šebela, 1998, Šebela et al., 2005, 2021; Novak, 2025), also observed in the MBGR cave (Fig. 4), were subsequently reactivated under changing conditions and stress regimes, producing brittle structures that could be used at different stages by speleogenesis.

Detailed analysis of the cave map, combined with field observations and tectonic measurements (Fig. 4), suggests that the passage from the main entrance to the central chamber, as well as numerous passages inside the cave, are aligned with the dominant Dinaric structural orientation (NW–SE; Figs. 4). At the cave entrance, a fissure of this orientation displays indications of a normal sense of movement, as inferred from the apparent displacement of bedding surfaces. In general, structures of this orientation were produced under Late Eocene NE-SW directed compression, driving the southwestward thrusting of the External Dinarides (Žibret and Vrabec, 2016); however kinematic indicators at the entrance to the cave suggest that these structures in the MGBR cave were later reactivated as normal faults during Early to Middle Miocene extension, linked to back-arc extension in the Pannonian Basin system (Žibret and Vrabec, 2016).

Within the MBGR cave, bedding planes dip gently to moderately toward the S-SW, similar to the direction observed in surface outcrops (Tyc et al., 2025). This trend remains consistent across all cave levels (Fig. 4) and appears to be followed by wide, low, gently to moderately tilted passages extending from the central part of the cave to the lower parts (Figs. 4 and profile used in Fig. 8). These passages appear to be preferentially developed along bedding surfaces or within interlayer spaces. The observed bedding tilting could be linked to NW-trending regional folds associated with NE-SW Cretaceous-Paleogene compression (Žibret and Vrabec, 2016), or to local rotation and tilting related to a W-E reverse fault that extends along the Sora River (Fig. 1).

The youngest deep shafts in the cave, identified by their N—S elongation and observed in the deepest and southernmost sections of the cave (Fig. 5), are controlled by N—S to NNE–SSW oriented faults and fractures. These structures are likely related to Pliocene-to-recent N—S compression, which resulted in dextral reactivation of regional-scale NW–SE faults bounding the study area (e.g., the Idrija and Ravne faults), accompanied by the development of N—S extensional fractures and mesofaults. This structural pattern corresponds to the present-day seismological activity (e.g., Čar, 2010; Žibret and Vrabec, 2016; Novak, 2025).

In summary, cave passages developed within dedolomites are predominantly controlled by Dinaric-oriented (NW–SE) fault zones and southward-inclined bedding planes. These structures correspond to NW–SE Dinaric faults and associated discontinuities that originally formed during Late Eocene NE–SW-directed compression and were subsequently reactivated as normal faults during Early to Middle Miocene extension. This structural framework suggests that dedolomitization and the main phase of phreatic cave development are most plausibly predated Miocene age and predate the formation of the youngest N–S-oriented, still vadose-active cave passages related to Pliocene–recent neotectonics.

5.3. Geochronological constraints on cave evolution based on speleothems and clastic sediments

Based on the geochronological data from speleothems and cave sediments, the cave's evolution can be subdivided into three main vadose stages. The earliest dated speleothem age is 380 ka, and together with the age of the unroofed Hleviše cave (420 ka), this suggests that by this time the cave had already been under vadose conditions for a considerable period. These ages correspond to the interglacial period after major Middle Pleistocene glaciation (480–430 ka) corresponding to MIS 12 or Mindel glaciation in the Alpine region (Hughes et al., 2010) and before Riss glaciation according to Alpine glacial nomenclature. Therefore, the initial phreatic conditions and dedolomitization must predate Middle Pleistocene based on geochronological data. Although no direct chronological data are available to constrain the timing of this process, the combined tectonic and geochronological evidence suggests that dedolomitization most likely occurred between the Miocene and the Middle Pleistocene.

Geochronological data from Prekova jama cave speleothem (PK in Fig. 1c), dated to 160–128 ka is particularly noteworthy because it formed during a glacial period corresponding to MIS 6 (Riss glaciation; Hughes et al., 2010), indicating that vadose conditions and speleothem deposition were present in the underground system at that time. The oldest non-fluvial sediments with bones of a cave bear (*Ursus spelaeus*) and the Middle Paleolithic cultural layers from the Matjaževe kamre cave are probably also from the end of this period (MK in Fig. 1c; Osole, 1976).

Cave sediments dated by OSL at 87 ka indicate that during this stage a specific sedimentary environment was established, characterized by allochthonous sediment input. This was most likely related to intensive surface erosion and sediment mobilization in a period in which vegetation cover was reduced under prevailing glacial conditions. Mineralogical analysis suggests that the sediment derives from Middle Triassic clastic units that are slightly younger and occur in contact with the cave-bearing dolostones, indicating a predominantly local sediment source. Based on granulometry and textural depositional characteristics this material can be classified as diamicton facies, likely introduced by debris-flow events, which supports a glacially influenced source of the sediment (Gillieson, 1986; Bosch and White, 2007; Robu et al., 2026). In

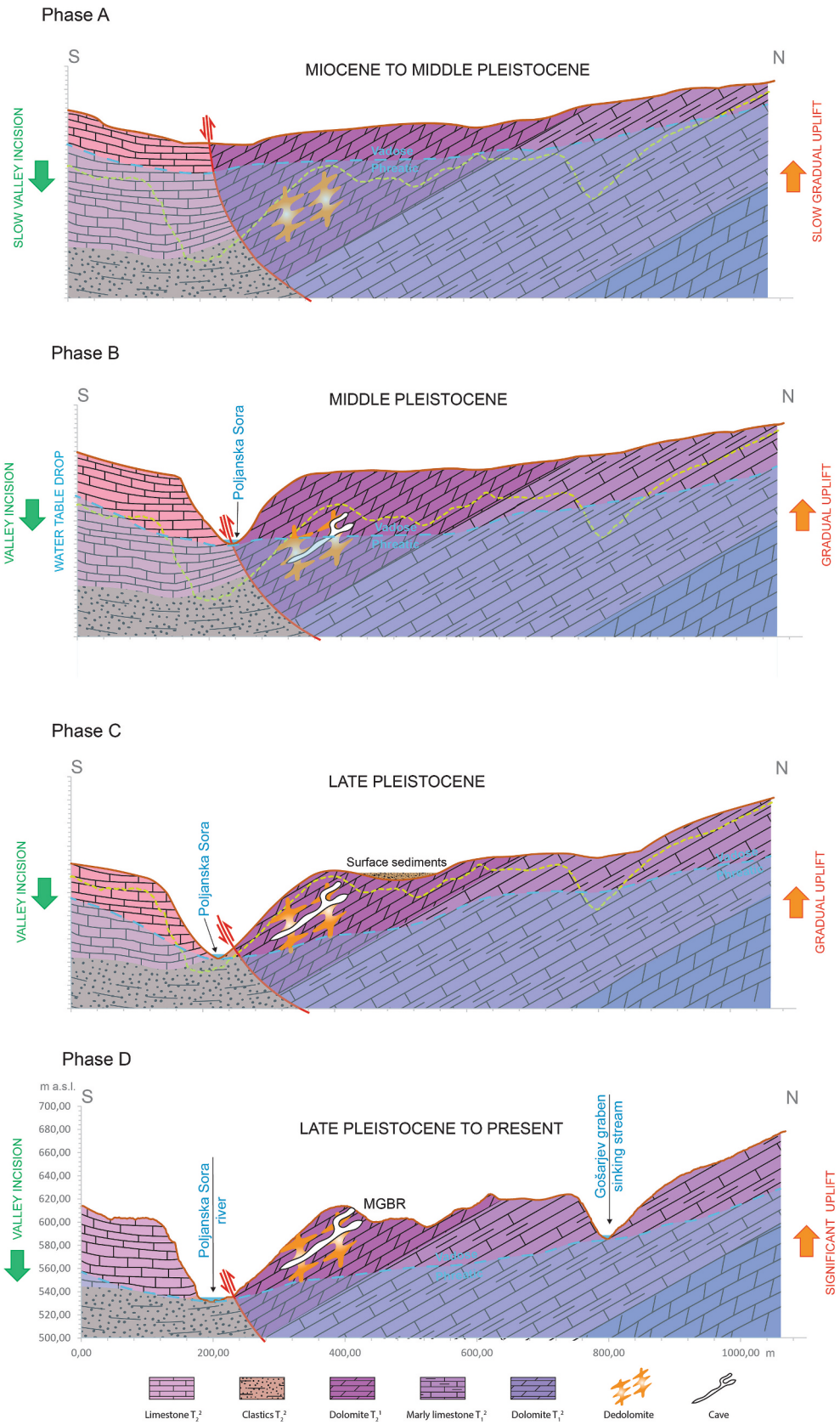

Fig. 10. Conceptual model of landscape evolution and cave development from the Miocene to the present along a south–north cross-section. Phase A shows speleogenetic conditioning under high base-level phreatic conditions, with dedolomitization along bedding planes and fractures. Phase B illustrates Middle Pleistocene interglacial uplift and valley incision, leading to groundwater-level lowering and epiphreatic to vadose conduit development. Phase C depicts continuous valley incision, maintaining dominantly vadose conditions. Phase D shows Late Pleistocene to present cave sediment deposition, renewed incision, sediment evacuation, vadose downcutting, speleothem growth, and ongoing modification.

addition to the matrix of debris-flow type sediment, fine-grained sediments of similar mineralogical composition occur as infill within wall and ceiling niches and cavities. Previous studies have shown that alluvial evolution, including sediment flux, incision, and aggradation during glacial–interglacial cycles, strongly influences karstification, local base level, and consequently speleogenesis (Harmand et al., 2017; Kurečić et al., 2021). This age is particularly interesting because it falls within MIS 5, encompassing the transition from the Eemian interglacial (MIS 5e) to the early Würm glaciation. The early Würm was characterized by pronounced climatic oscillations, including interstadial phases (MIS 5c and 5a) associated with glacier retreat and enhanced surface erosional and depositional activity (Milner et al., 2016).

Youngest geochronological data from MBGR are derived from the group of speleothems dated between 10 and 5 ka, corresponding to the Holocene period following the LGM (Würm glaciation; Hughes et al., 2010; Çiner et al., 2019).

5.4. Integrated model of cave evolution and landscape development

Based on the integration of geomorphological, structural, sedimentological, and geochronological data, we propose a multi-phase area development and cave-evolution model spanning from the pre-Middle Pleistocene to the present (Fig. 10). Dedolomitization occurred under high base-level phreatic conditions, when water with elevated Ca circulated along bedding planes and fracture networks producing porous, mechanically weakened zones that preconditioned the dolostone for later conduit development (Fig. 10; Phase A). This stage predates the Middle Pleistocene and, given the regional tectonic setting, may have occurred as early as the Miocene. Subsequent lowering of the base level led to shallower phreatic and progressively epiphreatic conditions, under which dedolomitization ceased and dissolution and erosion of both dolostone and dedolomite became the dominant process. These conditions promoted the initiation and early enlargement of proto-conduits within the previously weakened rock, marking a transitional phase between preconditioning and fully developed cave passage (Fig. 10; Phase B). Progressive tectonic uplift and valley incision before the Middle Pleistocene caused groundwater-level lowering and initiated structurally vadose conduit formation, as evidenced by Middle Pleistocene speleothem ages. During the Late Pleistocene, at least one phase of vadose sedimentation and antigravitative erosion was likely established, possibly dominated by debris-flow processes; these deposits were subsequently partially eroded during continued vadose conditions (Fig. 10; Phase C). Since the Late Pleistocene to Holocene, the system has remained dominantly vadose, with limited sediment input, with renewed speleothem growth, and ongoing modification driven by cave ventilation and condensation corrosion (Fig. 10; Phase D).

6. Conclusions

- The evolution of the MBGR cave system was fundamentally controlled by early-stage dedolomitization, which enhanced porosity, permeability, and structural weakness along fractures and bedding planes, acting as a key preconditioning process for speleogenesis
- Initial cave development preferentially exploited dedolomitized zones due to their higher dissolution potential relative to dolomite, and passage geometries partly reflect the spatial distribution and heterogeneity of dedolomite bodies
- Combined tectonic and geochronological evidence indicates that dedolomitization and the initial phreatic stages of cave development most likely occurred between the Miocene and the Middle Pleistocene.
- Progressive uplift and valley incision drove long-term transitions from phreatic to epiphreatic and ultimately vadose conditions, shaping cave evolution over at least the last 500 ka
- Most major cave passages formed prior to the Middle Pleistocene, whereas later climatic oscillations primarily controlled phases of speleothem growth and sediment input
- Since the Late Pleistocene, the cave has remained predominantly vadose, with sediment evacuation linked to ongoing uplift and river incision, and present-day morphology largely modified by condensation corrosion, particularly on dolostone walls
- The MBGR cave system demonstrates how cave morphologies, sediments, and speleothems constitute a valuable archive of landscape evolution, recording changes in surface erosion, sediment flux, and base-level development through time

CRediT authorship contribution statement

Filip Šarc: Writing – review & editing, Writing – original draft, Visualization, Methodology, Investigation, Formal analysis, Data curation, Conceptualization. **Andrzej Tyc:** Writing – review & editing, Writing – original draft, Visualization, Methodology, Investigation, Formal analysis, Data curation, Conceptualization. **Krzysztof Gaidzik:** Writing – review & editing, Writing – original draft, Visualization, Methodology, Investigation, Formal analysis, Data curation. **Marcin Błaszczyk:** Writing – review & editing, Methodology, Investigation, Formal analysis, Data curation. **Tanguy Racine:** Writing – review & editing, Writing – original draft, Visualization, Methodology, Investigation, Formal analysis, Data curation. **Matej Blatnik:** Methodology, Investigation, Formal analysis, Data curation. **Bojan Otoničar:** Writing – review & editing, Writing – original draft, Project administration, Methodology, Investigation, Funding acquisition, Formal analysis, Data curation, Conceptualization.

Declaration of competing interest

The authors declare that they have no known competing financial interests or personal relationships that could have appeared to influence the work reported in this paper.

Acknowledgements

This work was supported by the Slovenian Research and Innovation Agency (Research Programme Karst Research, No. P6-0119) and the National Science Center (NSC; Poland) through the bilateral Polish–Slovenian research project CEUS (project code in Slovenia: N1–0226; project code in Poland: 2020/39/I/ ST10/02357). Various equipment used for this work was funded by the EU Research Infrastructure projects RI-SI-LifeWatch, LifeWatch ERIC, and Implementation of the international infrastructure project LifeWatch + eLTER (I0-E016). We sincerely thank Dr. Jo De Waele for his very constructive comments, which significantly improved the quality of the manuscript and helped us to better exploit the LiDAR dataset. We also thank the Dr. Laurent Bruxelles, whose thoughtful comments strengthened the overall concept of the paper and improved the clarity of the interpretations.

Data availability

Data will be made available on request.

References

Al-Hashimi, W.S., Hemingway, J.E., 1973. Recent dedolomitization and the origin of the rusty crusts of Northumberland. J. Sediment. Petrol. 43, 82–91. https://doi.org/10.1306/74D726E9-2B21-11D7-8648000102C1865D.

Audra, P., Palmer, A.N., 2011. The pattern of caves: controls of epigenic speleogenesis. Géomorphologie : relief, processus, environnement 17, 359–378. https://doi.org/10.4000/geomorphologie.9571.

Audra, P., Palmer, A.N., 2015. Research frontiers in speleogenesis. Dominant processes, hydrogeological conditions and resulting cave patterns. Acta Carsol. 44. https://doi.org/10.3986/ac.v44i3.1960.

Back, W., Hanshaw, B.B., Plummer, N., Rahn, P.H., Rightmire, C.T., Rubin, M., 1983. Process and rate of dedolomitization: Mass transfer and ^{14}C dating in a regional carbonate aquifer. Geol. Soc. Am. Bull. 94, 1415–1429. https://doi.org/10.1130/0016-7606(1983)94%3C1415:PARODM%3E2.0.CO;2.

Bathurst, R.G.C., 1975. Carbonate Sediments and Their Diagenesis, 1st ed. Amsterdam.

Besl, P.J., McKay, N.D., 1992. Method for registration of 3-D shapes. In: Schenker, P.S. (Ed.), Sensor Fusion IV: Control Paradigms and Data Structures, pp. 586–606. https://doi.org/10.1117/12.57955.

Bischoff, J.L., Julia, R., Shanks, W.C., Rosenbauer, R.J., 1994. Karstification without carbonic acid: Bedrock dissolution by gypsum-driven dedolomitization. Geology 22, 995–998. https://doi.org/10.1130/0091-7613(1994)022%3C0995:KWCABD%3E2.3.CO;2.

Błaszczyk, M., Hercman, H., Pawlak, J., Szczygieł, J., 2021. Paleoclimatic reconstruction in the Tatra Mountains of the western Carpathians during MIS 9–7 inferred from a multiproxy speleothem record. Quat. Res. 99, 290–304. https://doi.org/10.1017/qua.2020.69.

Blatnik, M., Otoničar, B., 2018. Cave survey map of Mravljetovo brezno v Gošarjevih rupah (cave no. 7400). Cave Cadastre of Slovenia (Kataster jam Slovenije). Karst Research Institute ZRC SAZU, Postojna, Slovenia.

Bosch, R.F., White, W.B., 2007. Lithofacies And Transport Of Clastic Sediments In Karstic Aquifers. In: Studies of Cave Sediments. Springer Netherlands, Dordrecht, pp. 1–22. https://doi.org/10.1007/978-1-4020-5766-3_1.

Cantrell, D.L., Al-Khammash, A., Jenden, P.D., 2007. Characterization and significance of dedolomite in Wadi Nisah, central Saudi Arabia. GeoArabia 12 (3), 15–30. https://doi.org/10.2113/geoarabia120315.

Čar, J., 2010. Geological Structure of the Idrija - Cerkno hills. Explanatory book to the Geological map of the Idrija - Cerkljansko hills betiveen Stopnik and Rovte 1 : 25.000. Geological Survey of Slovenia, Ljubljana.

Čar, J., Gospodarič, R., 1983. O geologiji krasa med Postojno, Planino in Cerknico = About geology of karst among Postojna, Planina and Cerknica. Acta Carsologica 12, 91–105.

Çiner, A., Stepišnik, U., Sarıkaya, M.A., Žebre, M., Yıldırım, C., 2019. Last Glacial Maximum and Younger Dryas piedmont glaciations in Blidinje, the Dinaric Mountains (Bosnia and Herzegovina): insights from ^{36}Cl cosmogenic dating. Mediterranean Geoscience Reviews 1, 25–43. https://doi.org/10.1007/s42990-019-0003-4.

Columbu, A., Audra, P., Gázquez, F., D'Angeli, I.M., Bigot, J.-Y., Koltai, G., Chiesa, R., Yu, T.-L., Hu, H.-M., Shen, C.-C., Carbone, C., Heresanu, V., Nobécourt, J.-C., De Waele, J., 2021. Hypogenic speleogenesis, late stage epigenic overprinting and condensation-corrosion in a complex cave system in relation to landscape evolution (Toirano, Liguria, Italy). Geomorphology 376, 107561. https://doi.org/10.1016/j.geomorph.2020.107561.

Cooper, M.P., Covington, M.D., 2020. Modeling cave cross-section evolution including sediment transport and paragenesis. Earth Surf. Process. Landf. 45, 2588–2602. https://doi.org/10.1002/esp.4915.

D'Angeli, I.M., Parise, M., Vattano, M., Madonia, G., Galdenzi, S., De Waele, J., 2019. Sulfuric acid caves of Italy: a review. Geomorphology. https://doi.org/10.1016/j.geomorph.2019.02.025.

De Waele, J., Gutiérrez, F., 2022. Karst Hydrogeology, Geomorphology and Caves. Wiley. https://doi.org/10.1002/9781119605379.

De Waele, J., D'Angeli, I.M., Audra, P., Plan, L., Palmer, A.N., 2024. Sulfuric acid caves of the world: A review. Earth Sci. Rev. 250, 104693. https://doi.org/10.1016/j.earscirev.2024.104693.

Dreybrodt, W., Gabrovšek, F., Perne, M., 2016. Condensation Corrosion: A Theoretical Approach. Acta Carsologica 34 (2), 317–348. https://doi.org/10.3986/ac.v34i2.262.

Dubois, C., Quinif, Y., 2019. The ghost-rock of the chansin quarry (Belgium) – A remarkable example of pseudogallery. Geol. Belg. 22, 175–181. https://doi.org/10.20341/gb.2019.004.

Dubois, C., Quinif, Y., Baele, J.M., Barriquand, L., Bini, A., Bruxelles, L., Dandurand, G., Havron, C., Kaufmann, O., Lans, B., Maire, R., Martin, J., Rodet, J., Rowberry, M.D., Tognini, P., Vergari, A., 2014. The process of ghost-rock karstification and its role in the formation of cave systems. Earth Sci. Rev. 131, 116–148. https://doi.org/10.1016/j.earscirev.2014.01.006.

Evamy, B.D., 1967. Dedolomitization and the development of rhombohedral pores in limestones. J. Sediment. Petrol. 37, 1204–1215. https://doi.org/10.1306/74D71870-2B21-11D7-8648000102C1865D.

Flügel, E., 2004. Microfacies of Carbonate Rocks. Springer Berlin Heidelberg, Berlin, Heidelberg. https://doi.org/10.1007/978-3-662-08726-8.

Folk, R.L., 1965. Some Aspects of Recrystallization in Ancient Limestones. In: Dolomitization and Limestone Diagenesis. SEPM Society for Sedimentary Geology. https://doi.org/10.2110/pec.65.07.0014.

Ford, D.C., Williams, P.D., 2007. Karst Hydrogeology and Geomorphology, Revised edition. John Wiley & Sons, Chichester, UK (or Hoboken, NJ). https://doi.org/10.1002/9781118684986.

Gabrovšek, F., Häuselmann, P., Audra, P., 2014. 'Looping caves' versus 'water table caves': The role of base-level changes and recharge variations in cave development. Geomorphology 204, 683–691. https://doi.org/10.1016/j.geomorph.2013.09.016.

Gams, I., 2004. Kras v Sloveniji v prostoru in času, first ed. Založba ZRC SAZU, Ljubljana.

Gillieson, D., 1986. Cave sedimentation in the new Guinea highlands. Earth Surf. Process. Landf. 11, 533–543. https://doi.org/10.1002/esp.3290110508.

Girardeau-Montaut, D., 2016. CloudCompare.

Harmand, D., Adamson, K., Rixhon, G., Jaillet, S., Losson, B., Devos, A., Audra, P., 2017. Relationships between fluvial evolution and karstification related to climatic, tectonic and eustatic forcing in temperate regions. Quat. Sci. Rev. 166, 38–56. https://doi.org/10.1016/j.quascirev.2017.02.016.

Hauck, T.E., Corlett, H.J., Grobe, M., Walton, E.L., Sansjofre, P., 2018. Meteoric diagenesis and dedolomite fabrics in precursor primary dolomicrite in a mixed carbonate–evaporite system. Sedimentology 65, 1827–1858. https://doi.org/10.1111/sed.12448.

Hellstrom, J., 2003. Rapid and accurate U/Th dating using parallel ion-counting multi-collector ICP-MS. J. Anal. At. Spectrom. 18, 1346. https://doi.org/10.1039/b308781f.

Hellstrom, J., 2006. U–Th dating of speleothems with high initial 230Th using stratigraphical constraint. Quat. Geochronol. 1, 289–295. https://doi.org/10.1016/j.quageo.2007.01.004.

Hughes, P.D., Woodward, J.C., van Calsteren, P.C., Thomas, L.E., Adamson, K.R., 2010. Pleistocene ice caps on the coastal mountains of the Adriatic Sea. Quat. Sci. Rev. 29, 3690–3708. https://doi.org/10.1016/j.quascirev.2010.06.032.

Johnston, V.E., Šarc, F., Wątor, K., Otoničar, B., 2024. Hydrogeochemical data from carbonate springs as an aid for delimiting catchment areas in the Rovte region. Central Slovenia. J. Hydrol. Reg. Stud. 56, 102087. https://doi.org/10.1016/j.ejrh.2024.102087.

Kenny, R., 1992. Origin of disconformity dedolomite in the Martin Formation (Late Devonian, northern Arizona). Sediment. Geol. 78, 137–146. https://doi.org/10.1016/0037-0738(92)90117-A.

Klimchouk, A.B., 2009. Hypogene Speleogenesis and Karst Hydrogeology of Artesian Basins. In: Klimchouk, A.B., Ford, D.C. (Eds.), Principal Features of Hypogene Speleogenesis. Ukrainian Institute of Speleology and Karstology, Simferopol, pp. 7–15.

Klimchouk, A.B., Ford, D.C., Palmer, A.N., Dreybrodt, W., 2000. Speleogenesis: Evolution of Karst Aquifers, 1st ed. National Speleological Society, Inc., Huntsville, Alabama, USA.

Kukuljan, L., Gabrovšek, F., Covington, M.D., Johnston, V.E., 2021. CO2 dynamics and heterogeneity in a cave atmosphere: role of ventilation patterns and airflow pathways. Theor. Appl. Climatol. 146, 91–109. https://doi.org/10.1007/s00704-021-03722-w.

Kurečić, T., Bočić, N., Wacha, L., Bakrač, K., Grizelj, A., Tresić Pavičić, D., Lüthgens, C., Sironić, A., Radović, S., Redovniković, L., Fiebig, M., 2021. Changes in Cave Sedimentation Mechanisms During the Late Quaternary: An Example From the Lower Cerovačka Cave, Croatia. Front. Earth Sci. (Lausanne). 9, 672229. https://doi.org/10.3389/feart.2021.672229.

Liu, L., Wang, C., Huang, K., Du, Z., 2021. Petrography and origin of dedolomites of the Ordovician Majiagou formation in the southeastern Ordos Basin, China: implications for reservoir quality. Carbonates Evaporites 36 (4), 78. https://doi.org/10.1007/s13146-021-00741-6.

Mihevc, A., Gabrovšek, F., Knez, M., Kozel, P., Mulec, J., Otoničar, B., Petrič, M., Pipan, T., Prelovšek, M., Slabe, T., Šebela, S., Hajna, N., 2016. Karst in Slovenia. Karst in Slovenia. Bol. Geol. Min. 127, 79–97.

Milner, A.M., Roucoux, K.H., Collier, R.E.L., Müller, U.C., Pross, J., Tzedakis, P.C., 2016. Vegetation responses to abrupt climatic changes during the Last Interglacial Complex (Marine Isotope Stage 5) at Tenaghi Philippon, NE Greece. Quat. Sci. Rev. 154, 169–181. https://doi.org/10.1016/j.quascirev.2016.10.016.

Mlakar, I., 1969. Krovna zgradba Idrijsko Žirovskega ozemlja.

Mlakar, I., Čar, J., 2009. Geological map of the Idrija - Cerkno hills between Stopnik and Rovte 1 : 25.000.

Moska, P., Bluszcz, A., Poreba, G., Tudyka, K., Adamiec, G., Szymak, A., Przybyła, A., 2021. Luminescence Dating Procedures at the Gliwice Luminescence Dating Laboratory. Geochronometria 48, 1–15. https://doi.org/10.2478/geochr-2021-0001.

Nader, F.H., Swennen, R., Keppens, E., 2008. Calcitization/dedolomitization of Jurassic dolostones (Lebanon): Results from petrographic and sequential geochemical analyses. Sedimentology 55, 1467–1485. https://doi.org/10.1111/j.1365-3091.2008.00953.x.

Novak, U., 2025. Tectonic structures in karst: case studies from western Slovenia. PhD thesis,. University of Nova gorica, Nova Gorica, Slovenia, p. 168.

Osole, F., 1976. Matjaževe Kamre pleolitsko jamsko najdbišče. Arheol. Vestn. 13–34.

Otoničar, B., Dublyansky, Y., Osborne, R.A., Tyc, A., Philipp, S., 2016. Cave inception in dedolomite (a case study from central Slovenia). In: Chavez, T., Reehling, P. (Eds.), Proceedings of DeepKarst 2016: Origins, Resources, an Management of Hypogene Karst, NCKRI Symposium 6, 2016. National Cave and Karst Research Institute, Carlsbad, New Mexico.

Palmer, A.N., 2007. Cave Geology, 1st ed. Cave Books, Dayton, Ohio.

Pasini, G., 2009. A terminological matter: paragenesis, antigravitative erosion or antigravitational erosion? Int. J. Speleol. 38, 129–138. https://doi.org/10.5038/1827-806X.38.2.4.

Philipp, S., 2015. Hydrochemistry and Isotopic Analysis of Deep (Partly Thermal) Wells and Springs in NW-Slovenia. Master thesis, Universitäts-und Landesbibliothek Darmstadt. https://doi.org/10.13140/RG.2.2.19085.84966.

Placer, L., 2008. Principles of the tectonic subdivision of Slovenia. Geologija 51, 205–217. https://doi.org/10.5474/geologija.2008.021.

Racine, T., Trunz, C., Straubhaar, J., Jaillet, S., Renard, P., 2025. KarstConduitCatalogue: a dataset of LiDAR derived point clouds for the analysis of karstic conduit geometry and morphology. Earth Syst. Sci. Data 17, 4671–4690. https://doi.org/10.5194/essd-17-4671-2025.

Radwan, O.A., Dogan, A.U., Morsy, M.A., Kaminski, M.A., Humphrey, J.D., Christiansen, E.H., 2021. One-step versus two-step dolomite calcitization (dedolomitization): differences and inferences. Geosci. J. 25, 453–464. https://doi.org/10.1007/s12303-021-0004-8.

Raines, M.A., Dewers, T.A., 1997. Dedolomitization as a driving mechanism for karst generation in Permian Blaine Formation, southwestern Oklahoma, USA. Carbonates Evaporites 12, 24–31. https://doi.org/10.1007/BF03175799.

Robu, M., Tîrlă, M.-L., Mirea, I.-C., Faur, L.-M., Veres, D., Priceputu, A., Ungureanu, C., Vlaicu, M., Kenesz, M., Petculescu, A., Pourmand, A., Constantin, S., 2026. Hydroclimatic events in the Carpathian karst during MIS 3–2: evidence from sedimentary records in two Romanian caves. Sediment. Geol., 107104 https://doi.org/10.1016/j.sedgeo.2026.107104.

Ronchi, P., Jadoul, F., Savino, R., 2004. Quaternary dedolomitization along fracture systems in a Late Triassic dolomitized platform (Western Southern Alps, Italy). Carbonates Evaporites 19, 51–66. https://doi.org/10.1007/BF03175195.

Šarc, F., Powolny, T., Martín-Pérez, A., Košir, A., Gebus-Czupyt, B., Tyc, A., Ciesielczuk, J., Spötl, C., Koltai, G., Otoničar, B., 2025. Dedolomitization-driven karstification and speleogenesis in central Slovenia: Mineralogical and geochemical insights. Sediment. Geol. 490, 106986. https://doi.org/10.1016/j.sedgeo.2025.106986.

Šebela, S., 1998. Tektonska zgradba sistema Postojnskih jam / Tectonic structure of Postojnska jama cave system. ZRC SAZU, Založba ZRC (eng. ZRC publishing). https://doi.org/10.3986/961618265X.

Šebela, S., Gosar, A., Košťák, B., Stemberk, J., 2005. Active tectonic structures in the W part of Slovenia–Setting of micro-deformation monitoring net. Acta Geodyn. Geomater. 2, 45–57.

Šebela, S., Stemberk, J., Briestenský, M., 2021. Micro-displacement monitoring in caves at the Southern Alps–Dinarides–Southwestern Pannonian Basin junction. Bull. Eng. Geol. Environ. 80, 7591–7611. https://doi.org/10.1007/s10064-021-02382-4.

Stesky, R.M., 1998. SpheriStat user's manual.

Sznober, N., 2012. Cave survey map of Mravljetovo brezno v Gošarjevih rupah (cave no. 7400). Cave Cadastre of Slovenia (Kataster jam Slovenije). Karst Research Institute ZRC SAZU, Postojna, Slovenia.

Tucker, M.E., Wright, V.P., 1990. Carbonate Sedimentology. Wiley. https://doi.org/10.1002/9781444314175.

Tyc, A., Gaidzik, K., Šarc, F., Bania, D., Rządkowski, K., Otoničar, B., 2025. Morphostructural characteristics of the prealpine (isolated) karst: evidence from the Rovte region, Central Slovenia. In: Calux, A. (Ed.), 19th International Congress of Speleology Brasil, Belo Horizonte (Minas Gerais) July 20–27, 2025: Proceedings. Sociedade Brasileira de Espeleologia, São Paulo, pp. 110–114.

Vandeginste, V., John, C.M., 2012. Influence of climate and dolomite composition on dedolomitization: Insights from a multi-proxy study in the central Oman Mountains. J. Sediment. Res. 82, 177–195. https://doi.org/10.2110/jsr.2012.19.

Zeeh, S., Becker, F., Heggemann, H., 2000. Dedolomitization by meteoric fluids: the Korbach fissure of the Hessian Zechstein basin, Germany. J. Geochem. Explor. 69, 173–176. https://doi.org/10.1016/S0375-6742(00)00021-2.

Žibret, L., Vrabec, M., 2016. Paleostress and kinematic evolution of the orogen-parallel NW-SE striking faults in the NW External Dinarides of Slovenia unraveled by mesoscale fault-slip data anaysis. Geologia Croatica 69, 295–305. https://doi.org/10.4154/gc.2016.30.

Zupan Hajna, N., Pruner, P., Mihevc, A., Schnabl, P., Bosák, P., 2008. Cave sediments from Postojnska–Planinska Cave System (Slovenia): evidence of multi-phase evolution in epiphreatic zone. Acta Carsol. 37 (1), 63–86. https://doi.org/10.3986/ac.v37i1.160.